博士論文

Impaired synaptic function and social behavior induced by knockdown of autism spectrum disorder susceptibility genes in the mouse prefrontal cortex

(マウス前頭前野における自閉スペクトラム症感受性候補遺伝子のノックダウンによるシナプス機能と社会的行動の障害)

酒井　浩旭

Impaired synaptic function and social behavior induced by knockdown of autism spectrum disorder susceptibility genes in the mouse prefrontal cortex

(マウス前頭前野における自閉スペクトラム症感受性候補遺伝子のノックダウンによるシナプス機能と社会的行動の障害)

所属：　東京大学大学院医学系研究科機能生物学専攻神経生理学教室

指導教員：　狩野　方伸

申請者名：　酒井　浩旭

CONTENTS

Abstract

Autism spectrum disorder (ASD) is characterized by deficits in social interaction and communication, and stereotyped and repetitive behaviors. Recent studies have identified hundreds of genes whose mutations are found in patients with ASD. However, roles of these genes in synaptic function and ASD-like behaviors, causality between synaptic function and ASD-like behaviors, and key brain regions responsible for core symptoms of ASD remain poorly understood. Here I show that two ASD susceptibility genes, CNTNAP2 and AHI1, play critical roles in synapse function and ASD-like behaviors in mice, and that excitatory synaptic inputs regulated by these genes in layer II/III pyramidal neurons of the prefrontal cortex (PFC) are involved in ASD-like behaviors. Knockdown of CNTNAP2, which is implicated in synapse development and ASD, in the PFC showed impaired excitatory and inhibitory synaptic transmission, and ASD-like behaviors including reduced social interaction and communication. These results indicate that CNANAP2 in the PFC regulates synapse development and its disruption induces ASD-like behaviors and suggest that knockdown of genes in the PFC is utilized for identifying function-unknown ASD susceptibility genes. Using this system, I found that knockdown of the Abelson helper integration site-1 (AHI1), which is the first identified Joubert syndrome–associated gene and likely associated with ASD, in the PFC showed decreased excitatory synaptic transmission and ASD-like behaviors including reduced social interaction and communication. Moreover, treatment with CX546, a positive allosteric modulator of AMPA receptor, normalized excitatory synaptic transmission and improved social interaction in mice with AHI1-knockdown. These findings establish causality among genes, synaptic transmission and ASD phenotype, and emphasize the importance of excitatory synaptic transmission in the layer II/III pyramidal neurons of the PFC for ASD-like behaviors in mice.

Introduction

Autism spectrum disorder (ASD) includes a wide range of neurodevelopmental deficits and is diagnosed based on three criteria: deficits in social interaction and communication, and stereotyped and repetitive behaviors. Hundreds of genes associated with ASD have been identified (Abrahams and Geschwind, 2008; Devlin and Scherer, 2012). Because many of these genes encode synaptic proteins and mutations for several genes cause synaptic dysfunction and ASD-like behaviors in mice (Tabuchi et al., 2007; Peça et al., 2011; Won et al., 2012; Schmeisser et al., 2012), it has been hypothesized that synaptic dysfunction is one of the pathophysiological mechanisms of ASD (Delorme et al., 2013). However, key brain regions related to ASD are unknown and the causality between synaptic dysfunction and abnormal behavior associated with ASD remains unclear. Moreover, roles of many ASD-related genes in synapse function and ASD-like behaviors have not been investigated.

I focused on the prefrontal cortex (PFC) as a brain region which is presumed to be responsible for ASD-like behavioral abnormalities. The PFC has been implicated in the modulation of social behavior (Yizhar et al., 2011; Amodio and Frith, 2006; Courchesne et al., 2011; Liang et al, 2015) and children with autism have an abnormal excess number of neurons in the PFC (Courchesne et al., 2011). Disorders of the PFC development produce social defects in mice (Scearce-Levie et al., 2008) and optogenetic activation of the medial PFC (mPFC) neurons directly alters social behavior in adult mice (Yizhar et al., 2011). However, it remains unknown whether the disturbances of ASD susceptibility genes in the PFC from early developmental stage to adulthood impair synaptic function and cause ASD-like behaviors.

To reveal the roles of individual genes associated with ASD in synaptic development and function, and ASD-related behaviors in the PFC, and to examine the causality between synaptic dysfunction and abnormal behavior associated with ASD, an experimental system is required which enables us to examine easily and quickly the effects of deletions and mutations of candidate genes on synapses and behaviors. Contactin associated protein-like 2 (CNTNAP2) gene is a suitable gene for the development of such an experimental system. This gene encodes a member of the neurexin family that belongs to synaptic cell-adhesion molecules (Poliak et al., 1999 and Poliak et al., 2003). Many previous studies have reported that mutations in this gene are identified in ASD patients (Peñagarikano and Geschwind, 2012). CNTNAP2 knockout mice show abnormal neural network activity, ASD-like behavior including the triad of repetitive/restrictive behavior, impaired social interactions and communication (Penagarikano et al., 2011), reduced dendritic spine density (Varea et al., 2015) and altered inhibitory transmission in the hippocampal CA1 region (Jurgensen and Castillo, 2015). Knockdown of CNTNAP2 in cultured cortical neurons impairs development and function of synapses (Anderson et al., 2012). However, the contribution of the PFC for synaptic and behavioral phenotypes shown in CNTNAP2 knockout mice remains unknown.

In the first part of the present study, I knocked down CNTNAP2 gene in the mouse PFC during postnatal development to adulthood, examined the synaptic function in the PFC, and subjected the mice with CNTNAP2 knockdown to a battery of behavioral tests. Recently, methods using in utero electroporation and viruses which can examine the role of genes and specific brain regions in behaviors have been developed (Niwa et al., 2010； Wang et al., 2011; Kim et al., 2012; Li et al, 2013; Hayashi-Takagi et al.,

2014). I optimized these methods for synaptic function in the PFC and ASD, and aimed to establish an experimental system in which the effects of knockdown of certain ASD-associated gene in the mouse PFC on synaptic function and ASD-like behaviors can be assayed reliably and quickly. I found that knockdown of CNTNAP2 in the layer II/III pyramidal cells in the mouse PFC during postnatal development reduced the number of functional excitatory synapses as well as inhibitory synapses, and caused mild deficits in social interaction and communication. These results are largely consistent with those of the previous studies and suggest that CNTNAP2 is important for keeping normal number of functional synapses. Thus, the experimental system developed here can be used for evaluating the roles of other ASD-related genes in synaptic function and ASD-like behaviors.

In the second part of the present study, I used the experimental system established in the first part, and investigated Abelson helper integration site-1 (AHI1) gene as an ASD susceptibility gene whose function is unknown. This is one of the genes whose mutations are found in patients with Joubert syndrome, which is characterized by agenesis of the cerebellar vermis and mental retardation (Dixon-Salazar et al., 2004; Ferland et al., 2004). A significant proportion of patients with Joubert syndrome exhibit features of ASD (Holroyd et al., 1991; Ozonoff et al., 1999). Moreover, mutations in the AHI1 gene are encountered in ASD patients (Alvarez Retuerto et al., 2008). These data suggest that AHI1is involved in ASD, but the roles of AHI1 in synapse development and function, and a causal link between AHI1 gene and ASD phenotype remain unknown. I found that knockdown of AHI1 in the layer II/III pyramidal cells in the mouse PFC during postnatal development attenuated the postsynaptic AMPA receptor-mediated excitatory synaptic transmission, and caused mild deficits in social interaction and

communication. I also found that enhancing AMPA receptor-mediated excitatory transmission by the AMPA receptor positive allosteric modulator CX546 restored the synaptic dysfunction and impaired social interaction in the mice with AHI1 knockdown. These results suggest that AHI1 is important for normal AMPA-receptor-mediated excitatory transmission in the PFC and for ensuring normal social interaction.

Methods

Animals

ICR mice (SLC JAPAN) were used in the present study. All experiments were performed in accordance with the guidelines set down by the experimental animal ethics committees of the University of Tokyo and the Japan Neuroscience Society.

Preparation of vector constructs

Vectors were designed to express GFP, micro RNA (miRNA), and/or cDNA under the control of the CAG promoter (Niwa et al., 1991). The cDNA for CNTNAP2 or AHI1 was obtained by RT-PCR of a cDNA library from P1 and P30 mouse cortex. Each cDNA was subcloned into pCAG vectors. The BLOCK-iT Pol II miR RNAi expression vector kit (Invitrogen, CA, USA) was used for vector-based RNA interference (RNAi) analysis. The following engineered microRNAs were designed according to the BLOCK-iT Pol II miR RNAi Expression Vector kit guidelines (Invitrogen):

5’-TGCTGTGATCTAGGTGCCAAGGGTCAGTTTTGGCCACTGACTGACTGACC CTTCACCTAGATCA-3’ and

5’-CCTGTGATCTAGGTGAAGGGTCAGTCAGTCAGTGGCCAAAACTGACCCTT GGCACCTAGATCAC-3’ for CNATNAP2-microRNA-1;

5’-TGCTGTACAAGGTCAATCTCCACATTGTTTTGGCCACTGACTGACAATGTG

GATTGACCTTGTA-3’ and

5’-CCTGTACAAGGTCAATCCACATTGTCAGTCAGTGGCCAAAACAATGTGGA

GATTGACCTTGTAC-3’ for CNATNAP2-microRNA-2;

5’-TGCTGATAAGAAGCCAGCATCCTTCCGTTTTGGCCACTGACTGACGGAAG

GATTGGCTTCTTAT-3’ and

5’-CCTGATAAGAAGCCAATCCTTCCGTCAGTCAGTGGCCAAAACGGAAGGAT

GCTGGCTTCTTATC-3’ for CNATNAP2-microRNA-3;

5’-TGCTGTAGTGCTGAAGCTAAAGTGGAGTTTTGGCCACTGACTGACTCCAC

TTTCTTCAGCACTA-3’ and

5’-CCTGTAGTGCTGAAGAAAGTGGAGTCAGTCAGTGGCCAAAACTCCACTTT

AGCTTCAGCACTAC-3’ for CNATNAP2-microRNA-4;

5’-TGCTGATAAGATGAAACAGGACGTTCGTTTTGGCCACTGACTGACGAACG

TCCTTTCATCTTAT-3’ and

5’-CCTGATAAGATGAAAGGACGTTCGTCAGTCAGTGGCCAAAACGAACGTCC

TGTTTCATCTTATC-3’ for AHI1-microRNA-1;

5’-TGCTGTTGAATGGCAGGTCAGAGTACGTTTTGGCCACTGACTGACGTACT

CTGCTGCCATTCAA-3’ and

5’-CCTGTTGAATGGCAGCAGAGTACGTCAGTCAGTGGCCAAAACGTACTCTG ACCTGCCATTCAAC-3’ for AHI1-microRNA-2; 5’-TGCTGAACAGATGCGTACTCGAAGCTGTTTTGGCCACTGACTGACAGCTT CGAACGCATCTGTT-3’ and 5’-CCTGAACAGATGCGTTCGAAGCTGTCAGTCAGTGGCCAAAACAGCTTCGA GTACGCATCTGTTC-3’ for AHI1-microRNA-3. These oligonucleotides were subcloned into a CAG vector. The QuikChange lightning site-directed mutagenesis kit (Agilent Technologies, CA, USA) was used to generate RNAi-resistant forms of CNTNAP2 and AHI1 (CNTNAP2-rescue and AHI1-rescue), which harbor sense mutations (no alteration of amino acid codons). CNTNAP2-rescue was fused to mOrange2. AHI1-rescue was linked in-frame to mOrange2 interposed by a picornavirus “self-cleaving” P2A peptide sequence to enable efficient bicistronic expression. CNTNAP2-rescue and AHI1-rescue were subcloned into pCAG vectors. Scrambled control miRNA for CNTNAP2 and AHI1 was designed by shuffling the recognition region sequences. A BLAST search confirmed that the scrambled sequences had no target gene. All constructs were verified by DNA sequencing.

Five splice variants of CNTNAP2 are known to exist (Ensembl: http://asia.ensembl.org): Splice variant 1 (ENSMUST00000114641) is a full length

isoform (long form), whereas. splice valiant 2 (ENSMUST00000199100), 3 (ENSMUST00000150737) and 4 (ENSMUST00000060839) are short isoforms. Splice variant 5 (ENSMUST00000196561) does not contain an open reading protein. The CNATNAP2-microRNA-1 was designed to suppress the splice variant 1 (long form), 2 and 4 (short forms). The CNTNAP2-microRNA-2, 3 and 4 were designed to suppress the splice variant 1 (long form).

Two splice variants of AHI1 are known to exist (Ensembl: http://asia.ensembl.org): Splice variant 1 (ENSMUST00000105525) is a full length isoform (long form) whereas splice variant 2 (ENSMUST00000163505) is a short isoform (short form). The AHI1-microRNA-1 and 2 were designed to suppress the splice variant 1 (long form). The AHI1-microRNA-3 was designed to suppress the splice variant 1 (long form) and 2 (short form).

These CNTNAP2 and AHI1 microRNAs inhibited a well-characterized splice valiant (long form) for respective molecule (Poliak et al., 1999; Sheng et al., 2008), although it remains unknown to what extent the entire mRNA of each molecule is suppressed in neurons.

In utero electroporation

In utero electroporation was performed as described previously (Saito et al., 2006; Niwa et al., 2010). Pregnant mice at embryonic day (E) 14-15 were deeply anesthetized with an intraperitoneal injection of sodium pentobarbital (Somnopentil; Kyoritsu Seiyaku Co., Tokyo, Japan). Plasmids were dissolved in water. The plasmid vector, pCAG vectors, was used to knockdown the expression of CNTNAP2 and AHI1 in pyramidal cells. The plasmids were injected into either the left or right lateral ventricle, or bilateral ventricles with a glass micropipette. Electric pulses (35V for 50 ms, five-ten times at 950 ms intervals) were delivered via forceps-shaped electrodes (CUY650P5, Unique Medical Imada, Aichi, Japan) connected to an electroporator (CUY21, Nepa Gene,Chiba, Japan). Pups that expressed strong fluorescence in the prefrontal cortex of both hemispheres were used for behavior experiments.

Electrophysiological recordings from pyramidal cells in acute cortical slices

Coronal slices containing the mPFC (300 μm thick) were prepared from mice from P16 to P24 by using a vibratome slicer (Leica, Germany) in chilled (0 ºC-4 ºC) cutting solution of 120 mM Choline-Cl, 28mM $NaHCO_3$, 1.25 mM NaH_2PO_4, 2 mM KCl, 25 mM glucose, 1 mM $CaCl_2$, 8 mM $MgCl_2$, bubbled with 95% O_2 and 5% CO_2 (Narushima et al., 2006). The preparations were recovered for at least 30 min at room

temperature by incubation in a reservoir chamber bathed in a solution containing 125 mM NaCl, 2.5 mM KCl, 2 mM $CaCl_2$, 1 mM $MgSO_4$, 1.25 mM NaH_2PO_4, 26 mM $NaHCO_3$, and 20 mM glucose bubbled with 95% O_2 and 5% CO_2 (Uesaka et al., 2012; Uesaka et al., 2014). The preparations were transferred to a recording chamber located on the stage of an Olympus BX51WI microscope. Whole-cell recordings were made from visually identified or fluorescent protein-positive pyramidal cells using upright and fluorescence microscopes at 32ºC. The resistance of the patch pipettes was 2-4 MΩ when filled with an intracellular solution composing 120 mM $CsMeSO_3$, 15 mM CsCl, 8 NaCl, 0.2 mM EGTA, 10 mM HEPES, 10 mM TEA-Cl, 4 mM MgATP, 0.3 mM Na_2GTP, 0.1 mM Spermine, 5 mM Qx314 (pH7.3, adjusted with CsOH) for input-output relationship, paired pulse ratio, NMDA/AMPA experiments (Ding et al., 2011). A miniature EPSC (mEPSC) was measured with pipette solution containing 130 mM K D-gluconate, 6 mM KCl, 10 mM NaCl, 10 mM HEPES, 0.16 mM $CaCl_2$, 2 mM $MgCl_2$, 0.5 mM EGTA, 4 mM Na-ATP, and 0.4 mM Na-GTP (pH7.3, adjusted with KOH) (Maejima et al., 2005). A miniature IPSC (mIPSC) was measured with pipette solution containing 145 mM KCl, 10 mM HEPES, 5 mM ATP.Mg, 0.2 mM GTP-Na, 0.16 mM $CaCl_2$, 2 mM $MgCl_2$, and 10 mM EGTA (pH7.2, adjusted with KOH) (Ade et al., 2008). Membrane currents were recorded with an EPC-10 amplifier (HEKA

Elektronik, Lambrecht/Pfalz, Germany). The signals were filtered at 2.9 kHz and digitized at 20 kHz. The pipette access resistance was compensated by 70%.

Excitatory postsynaptic currents (EPSCs) were recorded from layer II/III pyramidal cells of the mPFC and stimulations were delivered by a bipolar tungsten stimulating electrode (FHC, Inc, USA) placed in layer II/III of the mPFC (Wang et al., 2011). The recording chamber was continuously perfused with oxygenated bath solution supplemented with picrotoxin (0.1 mM). The holding potential for recording EPSCs was -70mV. For measuring the paired-pulse ratio, double stimulation pulses were delivered through a single stimulation electrode at varying inter pulse intervals of 20 ms, 50 ms, 100 ms and 500 ms. 5-10 consecutive traces were averaged to obtain a mean EPSC trace. For measuring NMDA/AMPA ratio of evoked EPSCs, AMPA receptor-mediated and NMDA receptor-mediated EPSCs were recorded at holding potential of -70 mV and +50 mV, respectively. 20-30 consecutive traces were averaged to obtain a mean AMPA- or NMDA-EPSC trace. The amplitude of NMDA-EPSCs was measured 100 ms after the stimulus onset. mEPSC were recorded at -70 mV in the presence of 0.1 mM picrotoxin and 0.5 μM TTX. The decay time constant of mEPSC was measured by fitting the decay from the peak to 37% of the peak amplitude with, single exponential. mIPSC were recorded at -70 mV in the presence of 10 μM NBQX,

50 μM D-AP5 and 0.5 μM TTX. To examine the effects of knocking down CNTNAP2 and AHI1 in the mPFC, recordings were made from GFP-positive (knockdown) and GFP-negative cells (control) in the same slices.

To evaluate the effects of CX546 on synaptic phenotypes, mEPSC was collected before treatment with CX546. 200 μM CX546 was then added to the ACSF for at least 15 to 20 min, and mEPSC was measured in the presence of the drug.

Immunohistochemistry

Mice were deeply anesthetized with pentobarbital (100 μg/g of body weight, intraperitoneal injection), perfused with 4% paraformaldehyde (PFA) in 0.1 M phosphate buffer and then processed to obtain coronal microsliced sections (100 μm in thickness). After permeabilization (0.5% triton-X) and blockade of nonspecific binding (10% donkey serum), a rat anti-GFP antibody (1:1000; Nacalai Tesque, Kyoto, Japan) or a mouse anti-CaMKII antibody (1:200; Abcam, Cambridge, UK) was applied overnight at 4°C. After incubation with secondary antibodies for 4 hours at room temperature (an anti-rat IgG Alexa Fluor 488 antibody; 1:400, Life Technologies, Inc. or an anti-mouse Cy5 antibody; 1:300, Jackson), the immunolabeled sections were counterstained with DAPI (300 nM; Invitrogen, Life Technologies, Inc.) for nucleic acid

staining.

Evaluation of knockdown efficacy

The method has been described previously (Uesaka et al., 2012; Uesaka et al., 2014). HEK293T cells in a 24-well dish were transfected with an RNAi knockdown vector (CNTNAP2-knockdown, AHI1-knockdown), scramble vector (CNTNAP2-scr, AHI1-scr) and mOrange2-fused cDNA (CNTNAP2-mOrange, AHI1-mOrange) using X-tremeGENE 9 reagents. One day later, fluorescence signals from the cells were examined under a confocal laser scanning microscope (FV1200, Olympus).

Quantitative analysis of GFP-positive cells in cerebral cortex

To evaluate whether the distribution of transfected cells by in utero electroporation is located in the PFC, a GFP expression construct was incorporated in the bilateral ventricular zone at E14-E15. Serial coronal sections (from Bregma: +2.34 mm, +1.94 mm, +1.18 mm, +0.98 mm, and -1.34 mm) from adult mice (8-18 weeks) were obtained (Niwa et al., 2010). Images were acquired with a confocal laser scanning microscope (FV1200, Olympus). Fluorescence signals in medial prefrontal cortex (mPFC), dorsolateral prefrontal cortex (dl-PFC), orbitofrontal cortex (OFC), moter cortex (mCx),

sensory cortex (sCx), cingulate cortex (cgCx), retrosplenial cortex (rsCx), and other areas were calculated by using an image analysis software (ImageJ, NIH). A mouse brain atlas as a guide (The Mouse Brain in Stereotaxic Coordinates, second edition) was used to define these areas. The percentage of fluorescence signals of each area in relation to total intensity of all areas was calculated. In addition, for the dl-PFC and the mPFC, the percentage of the area containing GFP-positive cells relative to the entire area of the respective PFC subregion was measured.

To determine the transfection rate into pyramidal cells by in utero electroporation, the number of double-labeled cells for GFP (transfection marker) and CaMKII (marker for pyramidal cells) was counted in the regions of the PFC where GFP-positive cells were dense in layer II/III. Then the ratio of the number of double-labeled cells to that of CaMKII-positive cells was calculated.

Dendritic spine morphology

Dendritic spine morphology was examined as described previously (Dumitriu et al., 2011). GFP expression vectors (control) and GFP expression vectors containing the microRNA against AHI1 (AHI1 KD) were used. Images were acquired with a confocal laser scanning microscope (FV10i, Olympus) with 60 × oil-immersion

objective at zoom 4.1 as z series taken at 0.3-μm intervals (scan averaged, four times; 1,024 × 1,024 pixel resolution). Dendritic spines were analyzed quantitatively using Neurolucida software (MBF Bioscience, Williston, Vt., USA). The background intensity and the GFP signal intensity from dendrites were adjusted to the same levels between control and Ahi1 knockdown cells (mean gray value of the background; 9.55 ± 1.16 for control, 9.34 ± 1.45 for AHI KD. mean gray value of the dendrites; 253.55 ± 1.39 for control, 254.45 ± 0.14 for AHI KD). Boundary between the inside and outside of spine was determined such that regions with fluorescence intensity lower than 15% of the maximum GFP signal intensity were defined to be outside of spines. If spines were too packed, I turned to serial stack images and manually traced individual spines on dendrites. The density and head width of each spine was measured in layer II/III pyramidal cells of the mPFC.

Behavioral assays

All behavioral assays expect for the ultrasonic vocalization test were performed with age-matched adult male mice (8-18weeks). All behavior studies performed during light-on periods. Prior to all experiments, mice were acclimatized to the behavioral testing area for at least 60 min. CNTNAP2-scramble (control) and AHI1-scramble mice

(control) were used when compared with CNTNAP2-knockdown (CNTNAP2 KD) and AHI1-knockdown (AHI1 KD) mice, respectively.

Social novelty test

An open field apparatus (50 x 40 x 50 cm) was used for social novelty test as described previously (Takashima et al., 2011). In the first session of the test, two empty cylindrical wire cages (10 cm in diameter, 15 cm high) were located in two adjacent corners and a test mouse was placed in the open field for 10 min to habituate it. In the second session, a stranger mouse (adult male C57/B6, SLC JAPAN) was placed in one of the two wire cages and the other wire cage was kept empty (empty cage). Then, the test mouse was placed in the open field and allowed to freely explore the open field for 10 min. The two sessions were recorded by video and the times spent in the two corner squares (16.7×16.7 cm) containing the cages were measured with TimeOF4 software (O'Hara & Co., Japan). The cages were cleaned with water between each session.

Reciprocal social interaction test

Reciprocal social interaction test was performed as described previously (Gkogkas et al., 2013). Mice were placed in the corner of an open field (50 x 40 x 50 cm, 15 lux) and

adult male DBA2 mice (SLC JAPAN) were placed in the opposite corner. Behavior was recorded using a video camera located above of the open field for 5 min. Time spent physically contacting was analyzed automatically with TimeOF4 software (O'Hara & Co., Japan). Active contact number (which means that test mouse contact DBA2 mouse) was analyzed manually.

Ultrasonic vocalization (USV)

USV was tested as described previously (Tsai et al., 2012). Briefly, both male and female pups at P7 were isolated from their mother at random and gently placed into a container (plastic cylinder, 5 cm high, 5 cm in diamerer). USV was recorded for 5 min from the time of isolation. USV emission was monitored by an ultrasonic microphone (UltraSoundGate CM 16; Avisoft Bioacoustics, Berlin, Germany). The isolation container and microphone were placed in a sound attenuating box (63.5 x 42 x 37 cm). The microphone (sensitive to frequencies of 15 to 250 kHz) was connected to a personal computer with a sampling rate of 250 kHz in 16-bit format by Avisoft RECORDER (version 4.2.16; Avisoft Bioacoustics) via an USB recording interface (UltraSoundGate 116Hb; Avisoft Bioacoustics, Berlin, Germany).

Grooming behavior

Mice were placed in a transparent plastic cylinder (22 cm high, 12 cm in diamerer). After habituation for 5 min, mice grooming behavior was video recorded for 10min. Grooming time was measured.

Marble bury test

Marble bury test was performed as described previously (Santini et al., 2013). Twelve clear blue glass marbles (17 mm diameter), white paper bedding material (Shepherd Specialty Papers, Kalamazoo, MI) and transparent cages (20 x 11 x 12.5 cm) were used for this test. The cage was filled with bedding (5 cm depth) and 12 marbles were placed on the bedding surface spaced at about 4 cm intervals. The mice were placed into the cages and allowed to remain for 15 min. The number of marbles buried more than two-thirds in the bedding was counted.

Operant reversal learning

Operant chambers which consisted of two retractable levers and a pellet feeder, located in a sound attenuating box, was used for this test (Med-Associates Georgia, VT, USA). Two retractable levers were located symmetrically from the pellet feeder (i.e. Left and

right lever). Test consisted of two parts: training phase (day1-day5) and reversal phase (day6- day12). In the training phase, mice were trained to press the active lever to obtain the food pellet. One press on the active, but not inactive, lever resulted in feeding of one food pellet. Position of active or inactive lever was assigned randomly for individual mouse. Maximum of 20 food pellets were allowed during 20 min session. 4 sessions were repeated in one experimental day. In a reversal phase, the positions of active and inactive levers were swapped from the training phase. 4 session were repeated in one experimental day. The percentage of correct lever presses in relation to the total lever press was calculated. Through the experiment, mice were restricted in food intake to maintain their body weight 80 to 90% of free feeding body weight. Restriction of food intake began two days prior to training. Mice were weighed after daily sessions and fed an adjusted amount of food to maintain the target body weight. Water was available ad libitum throughout the experiment.

Elevated plus maze (EPM) test

EPM test was performed as described previously (Takashima et al., 2011). The EPM consisted of closed arms (25 × 5 × 15 cm (H)), open arms (25 × 5 × 0.5 cm (H)) and central platform of the maze (5 × 5 cm). It was elevated 50 cm above the floor and

placed in the light (200 lx). In the EPM test, mice were individually placed in the center area and allowed to move freely in the space for 10 min. % of time spent in the open arms, number of open arm and total distance traveled entries were measured. Data were collected and analyzed with TimeEP1 software (O'Hara & Co., Japan).

Light/Dark (LD) box test

LD box test was performed as described previously (Takashima et al., 2011). The apparatus consisted of light (250 lx) and dark chamber (20 × 20 × 25 (H) cm). There was an entrance which enabled mice to move across the light and dark chamber (3 × 5 cm). In the LD test, mice were individually introduced into the dark box and allowed to move freely in the LD box for 10 min. Time spent in the light box, latency to the first move into the light box, total distance traveled were measured. Data were collected and analyzed with TimeLD4 (O'Hara & Co., Japan).

Open filed test

Open filed test was performed as described previously (Takashima et al., 2011). Mice were placed in the open field apparatus (50 x 40 x 50 cm) with 15 lx. Mice were recorded with a video camera for 30 min, and total distance was calculated in 5 min

time bins with TimeOF4 software (O'Hara & Co., Japan).

Tail suspension test

Tail suspension test was performed as described previously (Kaidanovich-Beilin et al., 2009). Individual mice were suspended by their tails using self-adhesive tape from a small hook at one end of a perpendicular wire for 10 min. Mice behavior was recorded with a video camera. Duration of immobility was analyzed automatically with TimeFZ2 software (O'Hara & Co., Japan).

Forced swim test

Forced swim test was followed as described previously (Kaidanovich-Beilin et al., 2009). Mice were placed individually in a transparent plastic cylinder (22 cm high, 12 cm in diamerer), containing water at 25 ± 0.5 °C at a depth of 15 cm, and were forced to swim for 10 min. Mice behavior was recorded with a video camera. Duration of immobility was analyzed automatically with TimeFZ2 software (O'Hara & Co., Japan).

Y-maze test

Y-maze test was performed as described previously (Hatayama et al., 2011). Mice were

placed at the end of one arm with 200 lx and allowed to move freely throughout the maze during 7 min. The series of arm entries were analyzed automatically with TimeYM1 software (O'Hara & Co., Japan). If a mouse consecutively entries each of the three arms with no repetitions, I defined those situation as alternation. The percent alternation was calculated as: (number of alternations)/(total number of arm entries – 2)×100 (%).

Pharmacological rescue

CX546 (Sigma, USA) was dissolved in 25 % β-cyclodextrin (Nacalai Tesque, Kyoto, Japan) in water (Silverman et al., 2013). Intraperitoneal injection of CX546 (25 mg per kg) or vehicle (25 % β-cyclodextrin in water) was performed 30 min before the reciprocal social interaction test or 20 min before the social novelty test, considering 10 min habituation period in the latter test.

Statistical analysis

Data were expressed as the mean ± SEM. The Mann-Whitney *U* test was used to the electrophysiological and morphological data when two independent data sets were compared. For multiple comparisons, the Dunn test was used to the electrophysiological

and knockdown efficacy data. Student's *t*-test was used to the behavioral data. Differences between groups were judged to be significant when $P < 0.05$. All statistical analyses were performed using Graphpad Prism software (Graphpad software, San Diego, CA, USA).

Results

Effects of CNTNAP2-knockdown in layer II/III pyramidal cells of the PFC on synaptic function and ASD-like behaviors

I first aimed to establish a method to examine the roles of ASD susceptibility genes with unknown function in synaptic function and ASD-like behaviors. Although key brain regions responsible for ASD have not been clearly determined, previous studies indicate that the PFC is involved in behavioral abnormalities of ASD (Courchesne et al., 2011; Yizhar et al., 2011 ; Liang et al, 2015). Therefore, I focused on the PFC in the present study. Recent methods using in utero electroporation and viruses enable us to examine the role of genes and specific brain regions in behaviors (Niwa et al., 2010； Wang et al., 2011; Kim et al., 2012; Li et al, 2013; Hayashi-Takagi et al., 2014). By optimizing these protocols for synaptic function in the PFC and ASD, I tried to develop an assay system in which the effects of knockdown of certain ASD-associated gene in the mouse PFC on synaptic function and ASD-like behaviors can be assayed reliably and quickly. To elucidate the effectiveness of the assay system, one has to deal with an ASD-related gene whose roles in synaptic function and ASD-like behavior have been well characterized. I chose CNTNAP2, because knockdown of this gene has been shown to impair development and function of synapses in cultured neurons (Anderson et al., 2012) and CNTNAP2 null knockout mice have been shown to exhibit abnormal neural network activity, ASD-like behaviors (Penagarikano et al., 2011), decreased dendritic spine density (Varea et al., 2015) and altered hippocampal inhibition (Jurgensen and Castillo, 2015). I performed knockdown of CNTNAP2 gene by microRNA in the mouse PFC during postnatal development, and examined whether the CNTNAP2 gene

knockdown influenced synaptic function in the PFC and behaviors. By using the in utero electroporation technique (Saito, 2006), I transfected plasmids including EGFP and microRNAs against CNTNAP2 that were driven by the CAG promoter (Niwa et al., 1991) into pyramidal cells of the PFC at embryonic day 14-15. I confirmed that microRNAs against CNTNAP2 significantly reduced the expression of CNTNAP2 in human embryonic kidney (HEK) cells (Fig.1). I also verified that transfected cells at postnatal 8-18 weeks were layer II/III pyramidal neurons and were mainly located in the PFC, including dorsolateral prefrontal cortex (dl-PFC), medial prefrontal cortex (mPFC), orbitofrontal cortex (OFC), and anterior cingulate cortex (cgCX) (Fig.2a, b, d, e and 3). Percent of GFP-positive cells in the whole neuronal population was about 5% in the dl-PFC or the mPFC (Fig. 2c and f). To estimate how much percentage of layer II/III pyramidal neurons were transfected, I performed double immunostaining of the PFC for GFP (transfection marker) and CaMKII (marker for pyramidal cells) (Fig. 3a). I found that about 25% of CaMKII-positive layer II/III pyramidal cells expressed GFP in the PFC (Fig. 3b).

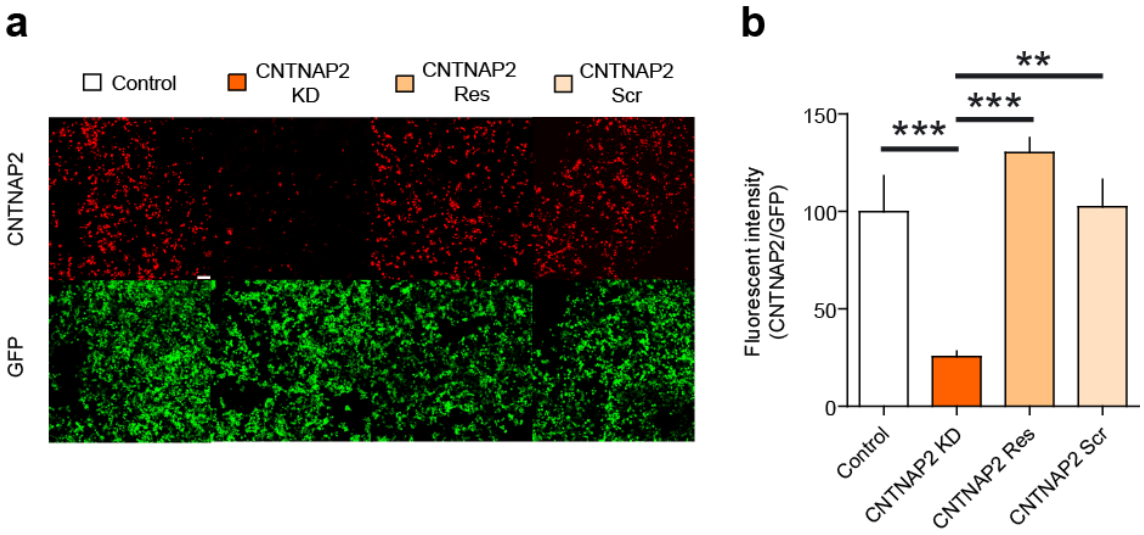

Figure 1 |Specificity and efficacy of the microRNA vectors for CNTNAP2-knockdown and CNTNAP2-rescue

a, Representative images for mOrange (red) and GFP (green) in HEK 293T cells transfected simultaneously with a CNTNAP2-mOrange and a GFP expression vectors (control), with the CNTNAP2-mOrange and the GFP expression vectors containing a microRNA against CNTNAP2 (CNTNAP2 KD), with an RNA interference (RNAi)-resistant CNTNAP2-mOrange vector and the GFP expression vector containing the microRNA against CNTNAP2 (CNTNAP2 Res), or with the CNTNAP2-mOrange and the GFP expression vectors containing a scramble microRNA against CNTNAP2 (CNTNAP2 Scr). Scale bar, 100 μm. **b,** Fluorescence intensity of mOrange relative to that of GFP in control (white column, n = 10), CNTNAP2 KD (deep orange columns, n = 10), CNTNAP2 Res (orange columns, n = 10), CNTNAP2 Scr (light orange columns, n = 11) cells. $^{**}P < 0.01$, $^{***}P < 0.001$ (Dunn test). Error bars show mean + SEM.

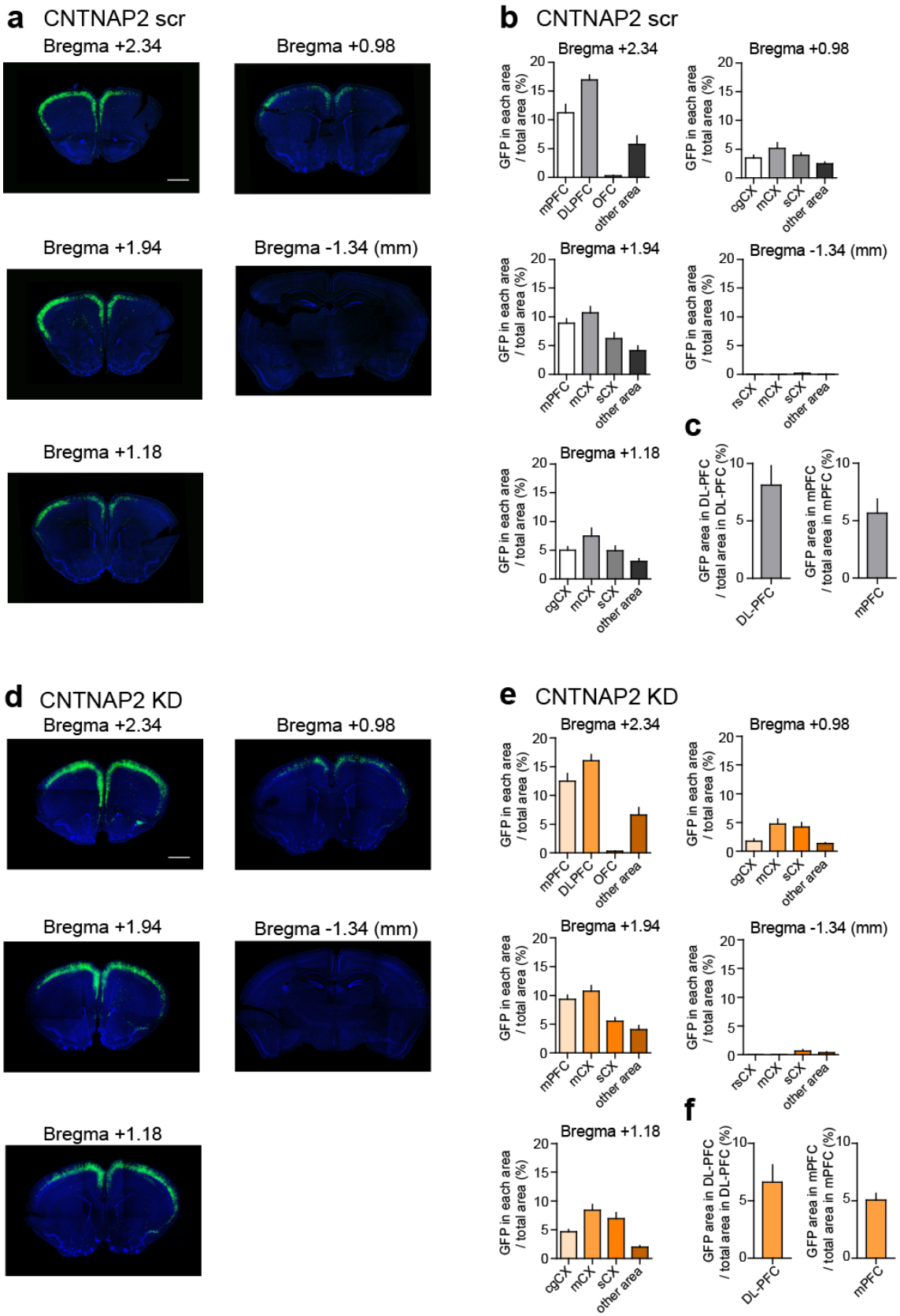
a CNTNAP2 scr
Bregma +2.34
Bregma +0.98
Bregma +1.94
Bregma -1.34 (mm)
Bregma +1.18
b CNTNAP2 scr
Bregma +2.34
Bregma +0.98
Bregma +1.94
Bregma -1.34 (mm)
Bregma +1.18
GFP in each area / total area (%)
mPFC
DLPFC
OFC
other area
cgCX
mCX
sCX
rsCX
c
GFP area in DL-PFC / total area in DL-PFC (%)
GFP area in mPFC / total area in mPFC (%)
DL-PFC
mPFC
d CNTNAP2 KD
e CNTNAP2 KD
f

Figure 2 | GFP-expressing transfected cells were localized in the PFC of mice that had undergone *in utero* electroporation of CNTNAP2-knockdown vectors

a, d, Representative rostro-caudal image series of coronal sections of brains (from Bregma: +2.34 mm, +1.94 mm, +1.18 mm, +0.98 mm, and -1.34 mm) with the GFP expression vectors containing the scramble microRNA against CNTNAP2 (CNTNAP2 Scr) (a) and the microRNA against CNTNAP2 (CNTNAP2 KD) (d). Blue, staining of nuclei. Scale bar, 1 mm. **b, e,** Quantification of distribution of GFP-positive cells in series of coronal sections of brains in CNTNAP2 Scr (b, n = 10) and CNTNAP2 KD (e, n = 10) slices. mPFC, medial prefrontal cortex; dl-PFC, dorsolateral prefrontal cortex; OFC, orbitofrontal cortex; cgCx, cingulate cortex; mCx, motor cortex; sCx, sensory cortex; rsCx, retrosplenial cortex. **c, f,** Proportion of the area containing GFP-positive cells in the dl-PFC and the mPFC relative to the entire area of respective PFC subregions in CNTNAP2 Scr (c, n = 10) and CNTNAP2 KD (f, n = 10) slices. Error bars show mean + SEM.

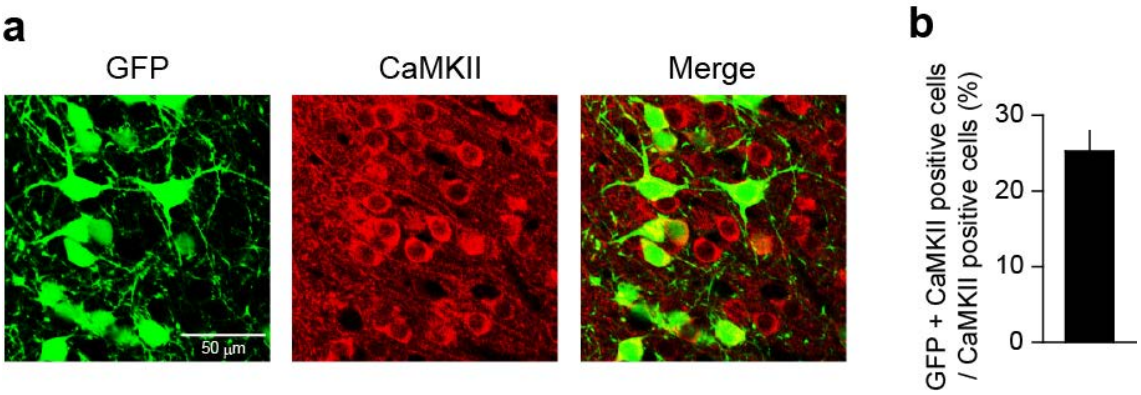

Figure 3 | Proportion of GFP-expressing transfected cells in CaMKII-positive layer II/III pyramidal cells of the PFC

a, Double immunostaining for GFP (green) and CaMKII (red) in layer II/IIII pyramidal cells of the PFC. GFP is expressed preferentially in CaMKII-positive pyramidal cells Scale bar, 50 μm. **b,** Proportion of GFP-expressing transfected cells in CNTNAP2 KD slices (n = 10) at postnatal day 21. Error bars show mean + SEM.

To examine the roles of CNTNAP2 in synapse function in the mPFC, I prepared coronal brain slices including the mPFC from the transfected mice at P16-P24, and made whole-cell patch-clamp recording from layer II/III pyramidal cells. I stimulated the layer II/III of the PFC about 50 μm away from the soma of recorded cells to evoke synaptic responses originating excitatory connections between layer II/III pyramidal cells (Fig. 4a). I compared the responses of GFP-positive CNTNAP2-knockdown cells with those of GFP-negative control cells. I found that the amplitude of excitatory postsynaptic currents (EPSCs) of CNTNAP2-knockdown cells were significantly smaller than those of control cells (Fig. 4b, c). I then recorded miniature excitatory postsynaptic current (mEPSC) and found that the frequency but not the amplitude was significantly lower in CNTNAP2-knockdown cells than in control cells (Fig. 4h-j). These results indicate that CNTNAP2-knockdown attenuated excitatory synaptic transmission either by the reduction of release probability and/or the number of release site in excitatory presynaptic terminals or by the increase in postsynaptically silent synapses. To check possible change in release probability, I examined paired-pulse ratio of evoked EPSCs. However, no difference was found in paired-pulse ratio between CNTNAP2-knockdown and control cells (Fig.4d, e). To check possible change in postsynaptic glutamate receptor function, I measured the ratio of AMPA receptor-mediated and NMDA receptor-mediated components of evoked EPSCs. However, no difference was found in NMDA/AMPA ratio between CNTNAP2-knockdown and control cells (Fig.4f, g). It is therefore concluded that the reduction in the number of release site is the most likely cause of the reduced excitatory transmission in CNTNAP2-knockdown cells. These results suggest that CNTNAP2-knockdown induces a reduction of functional excitatory synapses in layer

II/III pyramidal cells of the mPFC.

I then recorded miniature inhibitory postsynaptic current (mIPSC) to examine whether inhibitory synaptic transmission was altered by CNTNAP2 knockdown. The frequency but not the amplitude of mIPSC was significantly lower in CNTNAP2-knockdown cells than that in control cells (Fig. 4k-m), suggesting that CNTNAP2-knockdown decrease inhibitory synaptic transmission in layer II/III pyramidal cells of the mPFC. The effects of CNTNAP2-knockdown were rescued by co-injection of constructs for the expression of an RNAi-resistant CNTNAP2 (CNTNAP2 rescue) (Fig. 4b,c and h-m). Taken together, these results indicate that CNTNAP2 is required for normal excitatory and inhibitory synaptic function in pyramidal cells of the mPFC. These results are consistent with a previous study showing that knockdown of CNTNAP2 causes a significant reduction in excitatory and inhibitory synaptic responses in cultured cortical neurons (Anderson et al., 2012).

I next tested whether CNTNAP2-knockdown in the mouse PFC caused ASD-like behaviors. I first analyzed social interaction between two mice using a social novelty test. I compared the mice with CNTNAP2-knockdown with the control mice transfected with the scrambled sequence of the same nucleotide composition as the knockdown sequence in the PFC. Similar to the CNTNAP2 knockout mice reported previously (Peñagarikano et al., 2011), I found that the mice with CNTNAP2-knockdown in the PFC displayed a significant decrease in stay time with a stranger mouse cage compared with the control mice with CNTNAP2-scramble (Fig. 5a-d). To further examine social interaction, I performed the reciprocal social interaction test. I found that the mice with CNTNAP2-knockdown exhibited a significant reduction in the number of contact with another freely moving stranger mouse compared with the control mice (Fig. 5e, f).

These data indicate that the mice with CNTNAP2-knockdown in the PFC show impaired social interaction.

To examine whether anxiety contributed to the impairment of social interaction, I evaluated anxiety of mice using an elevated plus maze test and a light/dark box test. There was no change in anxiety-related behaviors between the mice with CNTNAP2-knockdown and with CNTNAP2-scramble (Fig. 6d-i). These results suggest that the impaired social interaction in the mice with CNTNAP2-knockdown is not likely due to an increase in anxiety.

I next tested whether communication among mice was impaired by CNTNAP2-knockdown. Mice pups use ultrasonic vocalization (USV) to communicate with their mothers. I analyzed USV at P7 and found that the mice with CNTNAP2-knockdown exhibited a significant reduction in the mean duration of calls compared with the control mice (Fig. 5g, h). This result suggests that the mice with CNTNAP2-knockdown in the PFC are mildly impaired in social communication.

ASD-like behaviors also include repetitive behavior and behavioral inflexibility. Excessive repetitive grooming and behavioral inflexibility have been shown in CNTNAP2 knockout mice (Peñagarikano et al., 2011). To test repetitive behaviors and behavioral flexibility, I measured self-grooming (repetitive behaviors), marble burying (repetitive behaviors), and operant reversal learning (behavioral flexibility) in the mice with CNTNAP2-knockdown in the PFC. However, I found no significant changes in these behaviors between the mice with CNTNAP2-knockdown and with CNTNAP2-scramble (Fig. 6a-c). These results suggest that repetitive behaviors and behavioral flexibility are not significantly affected by CNTNAP2 knockdown in layer II/III pyramidal neurons of the PFC. However, it should be noted that only about 25 %

of layer II/III pyramidal cells were transfected with CNTNAP2 knockdown vectors in the present experimental condition (Fig. 3). It is possible that the proportion of cells with CNTNAP2 knockdown may have been too small to cause discernible changes in repetitive behavior or behavioral inflexibility.

The traits of ASD often overlap with other disorders such as cognitive deficits, attention-deficit hyperactivity disorder and depression. To test the possibility of such complications, I used the Y-maze test (working memory), open filed test (locomotor activity), forced swim test (depression) and tail suspension test (depression). The mice with CNTNAP2-knockdown exhibited increased depressive trait but normal locomotor activity and working memory compared with the control mice with CNTNAP2-scramble (Fig. 6j-o).

The results so far indicate that CNTNAP2-knockdown in layer II/III pyramidal cells of the mouse PFC reduces their excitatory and inhibitory synaptic transmission, and that the synaptic dysfunction in the PFC leads to ASD-like behaviors. Since these results are largely consistent with those reported previously in CNTNAP2-knockdown neurons and CNTNAP2-knockout mice, the assay system can be used to evaluate the roles of other ASD-related genes in synaptic function and in ASD-like behaviors.

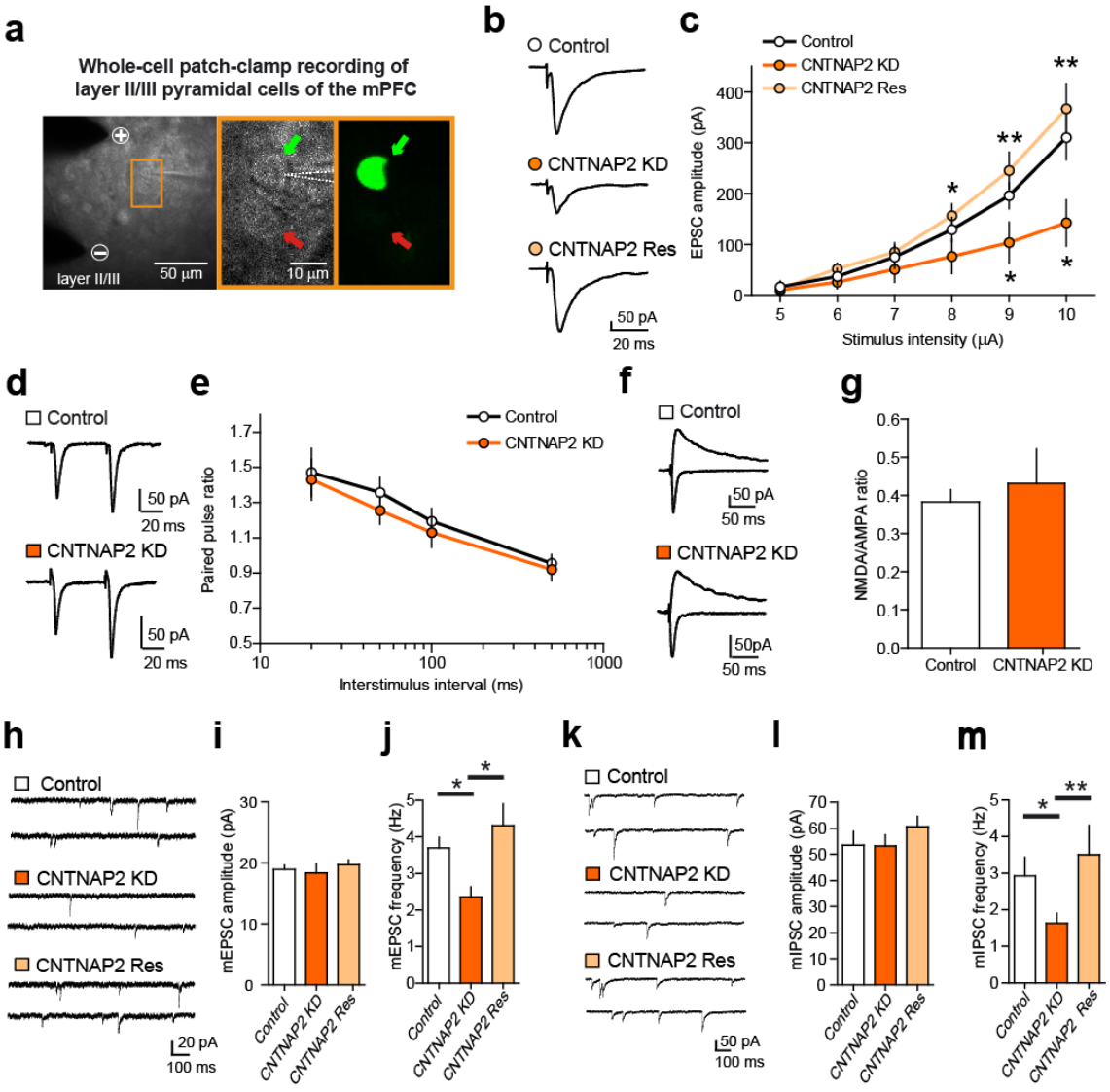

Figure 4 | Effects of CNTNAP2-knockdown in layer II/III pyramidal cells of the mPFC on synaptic function.

a, Representative images of recorded pyramidal cells. Dashed white lines delineate a patch pipette. + and - show the anode and the cathode, respectively, of tungsten stimulus electrodes. Middle and right panels are bright field (middle) and fluorescent (right) images of the portion indicated with orange rectangle in the left panel. Green and red arrows represent an EGFP-positive knockdown cell and an EGFP-negative control cell, respectively. **b, c,** Representative traces (b) and the averaged input-output relationships (c) for EPSCs induced by stimulation in the layer II/III of the mPFC in control (white circles, n = 13), CNTNAP2-knockdown (CNTNAP2 KD) (orange circles, n = 13) and CNTNAP2-rescue (CNTNAP2-Res) (light orange circles, n = 11) pyramidal cells. The holding potential was -70 mV. *P < 0.05, **P < 0.01 (Dunn test). **d, e,** Representative

traces (d) and the averaged paired-pulse ratio (e) for control (white circles, n = 12) and CNTNAP2-knockdown (CNTNAP2 KD) (orange circles, n = 10) pyramidal cells. **f, g,** Representative traces (f) and the averaged NMDA/AMPA ratio (g) for control (white columns, n = 13) and CNTNAP2-KD, (orange columns, n = 10) cells. No significant difference (Mann-Whitney U test). **h-j,** Sample traces of mEPSC (h) and summary bar graphs showing the mean amplitude (i) and frequency (j) of mEPSC for control (white columns, n = 14), CNTNAP2 KD (orange columns, n = 14) and CNTNAP2 Res (light orange columns, n = 13) cells. **k-m,** Sample traces of mIPSC (k) and summary bar graphs showing the mean amplitude (l) and frequency (m) of mIPSC for control (white columns, n = 19), CNTNAP2 KD (orange columns, n = 19) and CNTNAP2 Res (light orange columns, n = 15) cells. $*P < 0.05$, $**P < 0.01$ (Dunn test). Error bars show mean ± SEM.

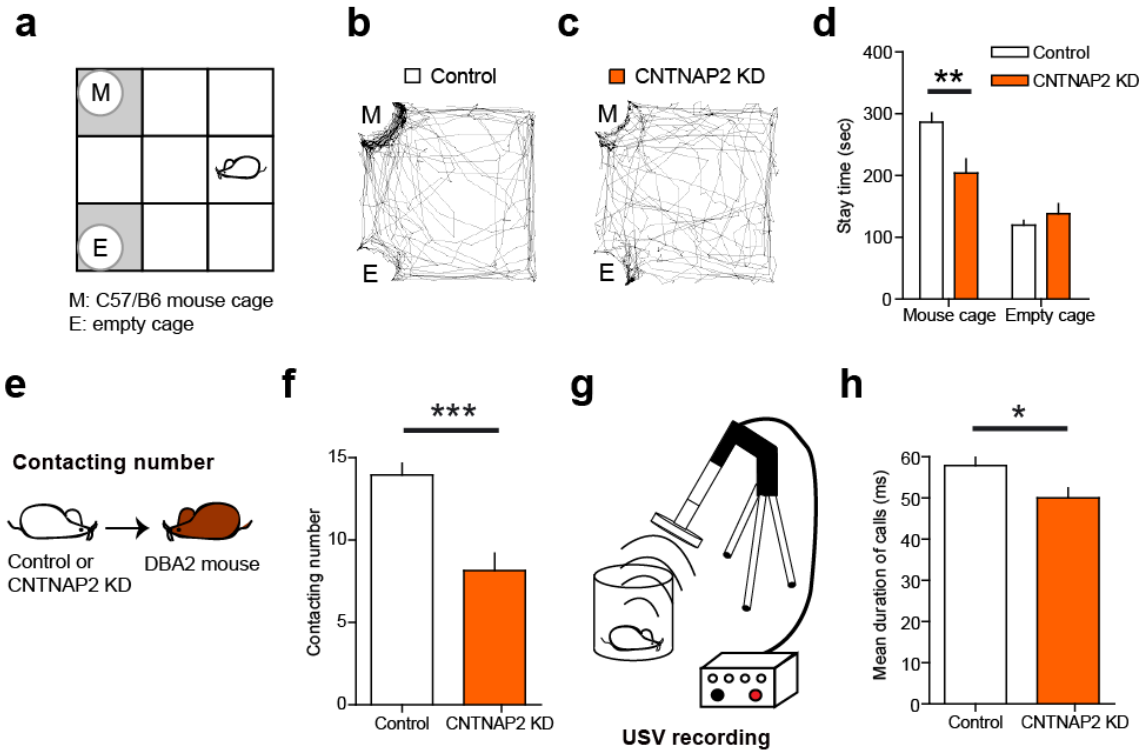

Figure 5 | Effects of CNTNAP2-knockdown in layer II/III pyramidal cells of the PFC on ASD-like behaviors.

a-h, Schema of social novelty test (a). Representative tracks (b, c) and quantification (d) of the results in j and k, as shown by the amount of time spent around the mouse (M) and empty cage (E) for CNTNAP2-scramble (control) (white columns, n = 23) and CNTNAP2 KD (orange columns, n = 20) mice. $^{**}P < 0.01$ (Student's *t* test). **e, f,** Schema of social reciprocal interaction test (e). Number of contacts (f) for control (white column, n = 22) and CNTNAP2 KD (orange column, n = 19) mice. $^{***}P < 0.001$ (Student's *t* test). **g, h,** Schema of USV test (g). Mean duration of calls (h) for control (white columns, n = 16), CNTNAP2 KD (orange columns, n = 14) pups. $^{*}P < 0.05$ (Student's *t* test). Error bars show mean ± SEM.

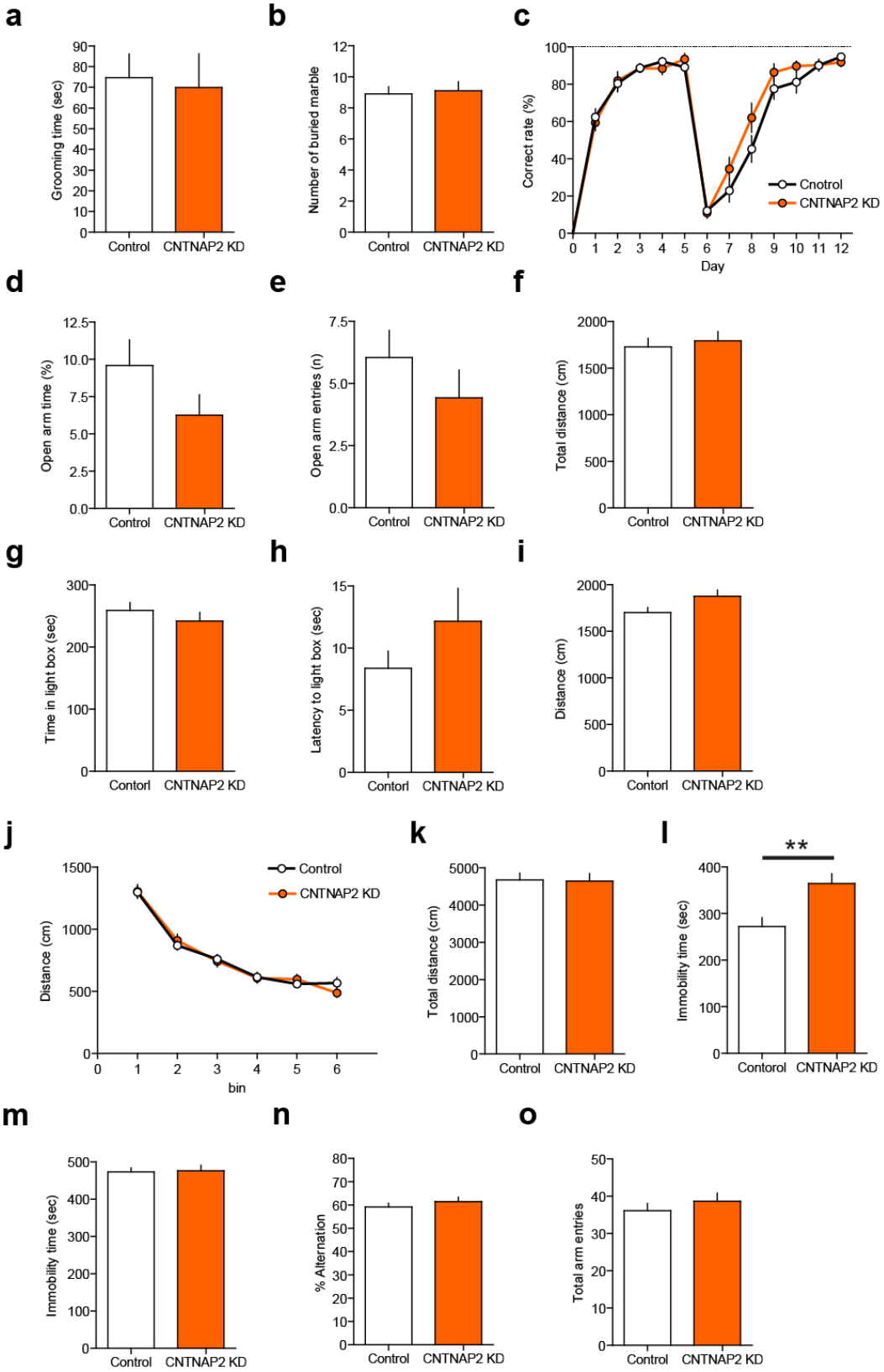
a
Grooming time (sec)
Control
CNTNAP2 KD
b
Number of buried marble
Control
CNTNAP2 KD
c
Correct rate (%)
Day
Cnotrol
CNTNAP2 KD
d
Open arm time (%)
Control
CNTNAP2 KD
e
Open arm entries (n)
Control
CNTNAP2 KD
f
Total distance (cm)
Control
CNTNAP2 KD
g
Time in light box (sec)
Contorl
CNTNAP2 KD
h
Latency to light box (sec)
Contorl
CNTNAP2 KD
i
Distance (cm)
Contorl
CNTNAP2 KD
j
Distance (cm)
bin
Control
CNTNAP2 KD
k
Total distance (cm)
Control
CNTNAP2 KD
l
**
Immobility time (sec)
Contorol
CNTNAP2 KD
m
Immobility time (sec)
Control
CNTNAP2 KD
n
% Alternation
Control
CNTNAP2 KD
o
Total arm entries
Control
CNTNAP2 KD

Figure 6 | Normal repetitive behaviors, behavioral flexibility, anxiety, locomotor activity and working memory but moderately enhanced depressive behavior in mice with CNTNAP2-knockdown in the PFC.

a, Self-grooming test. Total time spent on grooming in control (white column, n = 22) and CNTNAP2 KD (orange column, n = 19) mice. **b,** Marble bury test. Number of buried marbles in control (white column, n = 22) and CNTNAP2 KD (orange column, n = 19) mice. **c,** Operant reversal learning. Correct rate in control (white column, n = 18) and CNTNAP2 KD (orange column, n = 12) mice. **d-f,** Elevated plus maze test. Percentage of time in the open arm (d), the number of open arm entries (e) and total distance travelled (f) for control (white column, n = 22) and CNTNAP2 KD (orange column, n = 19) mice. **g-i,** Light/Dark box test. Time in the light box (g), latency to the light box entry (h), and distance travelled (i) for control (white column, n = 22) and CNTNAP2 KD (orange column, n = 19) mice. **j,k,** Open field test. Total distance travelled shown in 5 min time bins (j) and during 30 min (k) for control (white column, n = 23) and CNTNAP2 KD (orange column, n = 20) mice. **l,** Tail suspension test. Immobility time in control (white column, n = 22) and CNTNAP2 KD (orange column, n = 19) mice. **m,** Forced swim test. Immobility time in control (white column, n = 22) and CNTNAP2 KD (orange column, n = 19) mice. **n,o,** Y-maze test. Percentage of alternation in control (white column, n = 22) and CNTNAP2 KD (orange column, n = 19) mice. $^{**}P < 0.01$ (Student's *t* test). Error bars show mean ± SEM.

AHI1-knockdown decreases excitatory synaptic transmission in layer II/III pyramidal cells of the PFC

Next, I examined *AHI1*, an ASD-related gene with unknown function, by using the assay system newly developed in the present study. Mutation in AHI1 gene is one of the causes of Joubert syndrome characterized by agenesis of the cerebellar vermis, cognitive impairment and delayed development (Dixon-Salazar et al., 2004; Ferland et al., 2004). About 30% of patients with Joubert syndrome have ASD (Ozonoff et al., 1999). In addition, common genetic variation in AHI1 is associated with ASD (Alvarez Retuerto et al., 2008). These findings suggest that AHI1 disruption may lead to symptoms of ASD. However, the involvement of AHI1 in synapse function in the PFC and the link between AHI1 disruption and ASD remain unclear. To evaluate the effects of AHI1 deficiency in synapse development and function as well as ASD-like behaviors, I knocked down AHI1 in pyramidal cells of the mouse PFC during postnatal development. I confirmed that microRNAs against AHI1 significantly reduced the expression of AHI1 in HEK cells (Fig. 7). I also verified that the transfected cells were layer II/III pyramidal cells and mainly located in the PFC (Fig. 8a, b, d and e). Percent of GFP-positive cells in the whole neuronal population was about 2 to 8% in the dl-PFC or the mPFC (Fig. 8c and f).

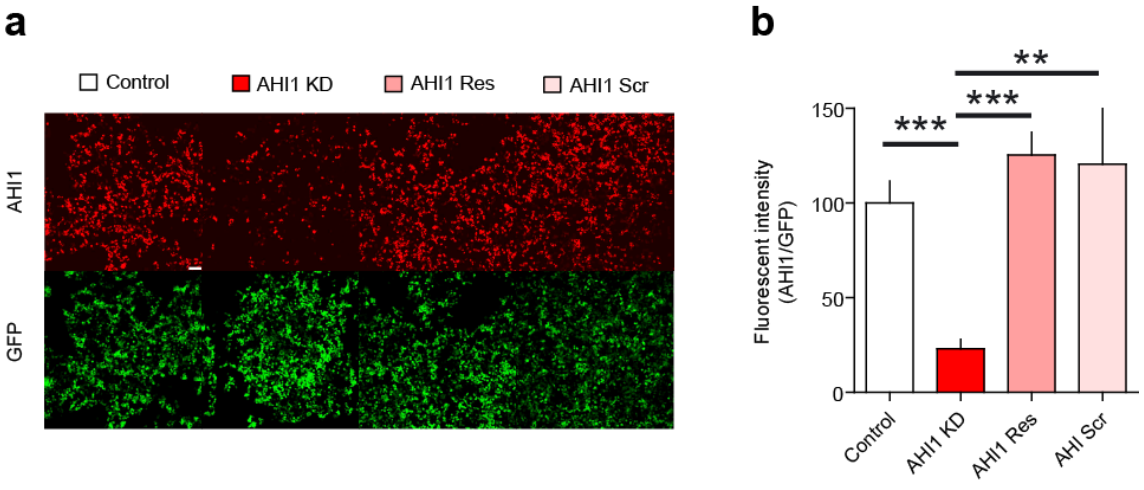

Figure 7 | Specificity and efficacy of the microRNA vectors for AHI1-knockdown and AHI1-rescue

a, Representative images for mOrange (red) and GFP (green) in HEK 293T cells transfected simultaneously with an AHI1-mOrange and a GFP expression vectors (control), with the AHI1-mOrange and the GFP expression vectors containing an microRNA against AHI1 (AHI1 KD), with an RNA interference (RNAi)-resistant AHI1-mOrange vector and the GFP expression vectors containing the microRNA against AHI1 (AHI1 Res), or with the AHI1-mOrange and the GFP expression vectors containing a scramble microRNA against AHI1 (AHI1 Scr). Scale bar, 100 μm. **b,** Fluorescence intensity of mOrange relative to that of GFP in control (white column, n = 11), AHI1 KD (deep orange columns, n = 10), AHI1 Res (orange columns, n = 10), AHI1 Scr (light orange columns, n = 13) cells. $^{**}P < 0.01$, $^{***}P < 0.001$ (Dunn test). Error bars show mean + SEM.

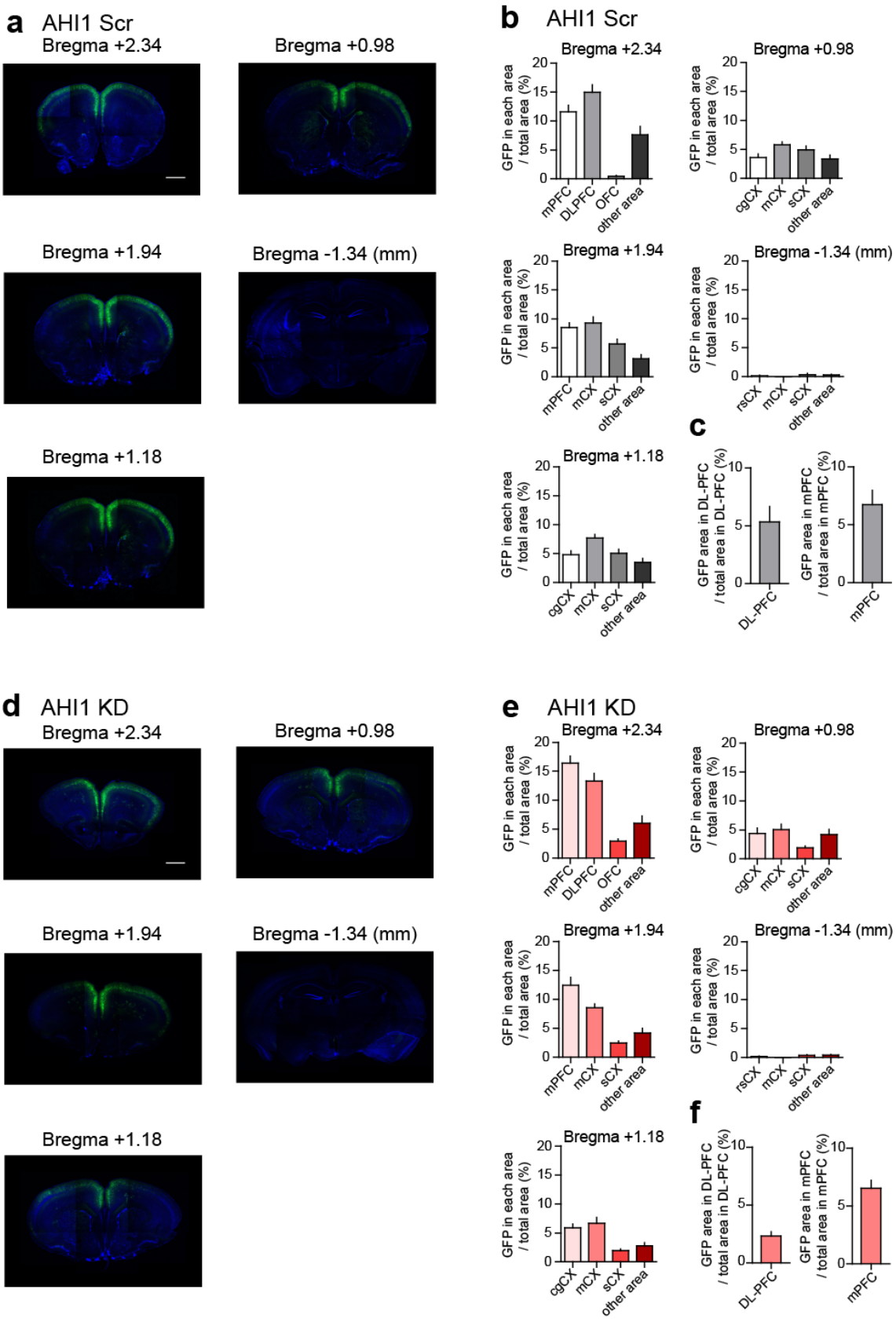
a
AHI1 Scr
Bregma +2.34
Bregma +0.98
Bregma +1.94
Bregma -1.34 (mm)
Bregma +1.18
b
AHI1 Scr
Bregma +2.34
Bregma +0.98
Bregma +1.94
Bregma -1.34 (mm)
Bregma +1.18
GFP in each area / total area (%)
mPFC
DLPFC
OFC
other area
cgCX
mCX
sCX
rsCX
c
GFP area in DL-PFC / total area in DL-PFC (%)
GFP area in mPFC / total area in mPFC (%)
DL-PFC
mPFC
d
AHI1 KD
Bregma +2.34
Bregma +0.98
Bregma +1.94
Bregma -1.34 (mm)
Bregma +1.18
e
AHI1 KD
Bregma +2.34
Bregma +0.98
Bregma +1.94
Bregma -1.34 (mm)
Bregma +1.18
f

Figure 8 | GFP-expressing transfected cells were localized in the PFC of mice that had undergone *in utero* electroporation of AHI1-knockdown vectors

a, d, Representative rostro-caudal image series of coronal sections of brains (from Bregma: +2.34 mm, +1.94 mm, +1.18 mm, +0.98 mm, and -1.34 mm) with the GFP-expression vectors containing the scramble microRNA against AHI1 (AHI1 Scr) (a) and the microRNA against AHI1 (AHI1 KD) (c). Blue, staining of nuclei. Scale bar, 1 mm. **b, e,** Quantification of distribution of GFP-positive cells in series of coronal sections of brains in AHI1 Scr (b, n = 10) and AHI1 KD (e, n = 10) slices. mPFC, medial prefrontal cortex; dl-PFC, dorsolateral prefrontal cortex; OFC, orbitofrontal cortex; cgCx, cingulate cortex; mCx, motor cortex; sCx, sensory cortex; rsCx, retrosplenial cortex. **c, f,** Proportion of the area containing GFP-positive cells in the dl-PFC and the mPFC relative to the entire area of respective PFC subregions in AHI1 Scr (c, n = 10) and AHI1 KD (f, n = 10) slices. Error bars show mean ± SEM.

I then examined roles of AHI1 in synaptic function of layer II/III pyramidal cells in the mPFC. I recorded EPSCs evoked by layer II/III stimulation in acute slices prepared from mice at P16-P24 that had undergone in utero electroporation of vectors at E14-E15. I found that the amplitude of evoked EPSCs of AHI1-knockdown cells were significantly smaller than those of control cells (Fig. 9a, b). Furthermore, the NMDA/AMPA ratio was significantly larger in AHI1-knockdown pyramidal cells than in control cells (Fig. 9c, d). The amplitude but not the frequency of mEPSC was significantly smaller in AHI1-knockdown cells than in control cells (Fig. 9e-g). There was no difference in paired-pulse ratio of evoked EPSC between AHI1-knockdown and control cells (Fig. 10a, b). These data suggest that AHI1-knockdown reduced postsynaptic sensitivity but did not affect either the number of release site or the release probability at excitatory presynaptic terminals. As for inhibitory synaptic transmission, no significant difference was noted in the amplitude and the frequency of mIPSC between AHI1-knockdown and control cells (Fig. 10c-e). These effects of AHI1-knockdown were rescued by co-injection of the RNAi-resistant AHI1 (AHI1 rescue) (Fig. 9). These results suggest that AHI-knockdown leads to a specific reduction of postsynaptic responsiveness at excitatory synapses in layer II/III pyramidal cells of the mPFC. Since excitatory postsynaptic responses are dependent on the shape of dendritic spines on which glutamatergic terminals form excitatory synapses, I tested whether AHI1-knockdown caused any change in spine morphology. While the spine density was not affected, the spine head width was significantly decreased in AHI1-knockdown cells compared with control cells (Fig. 10f-h). This change in spine morphology is presumably a cause of the reduced excitatory synaptic transmission in AHI1-knockdown cells.

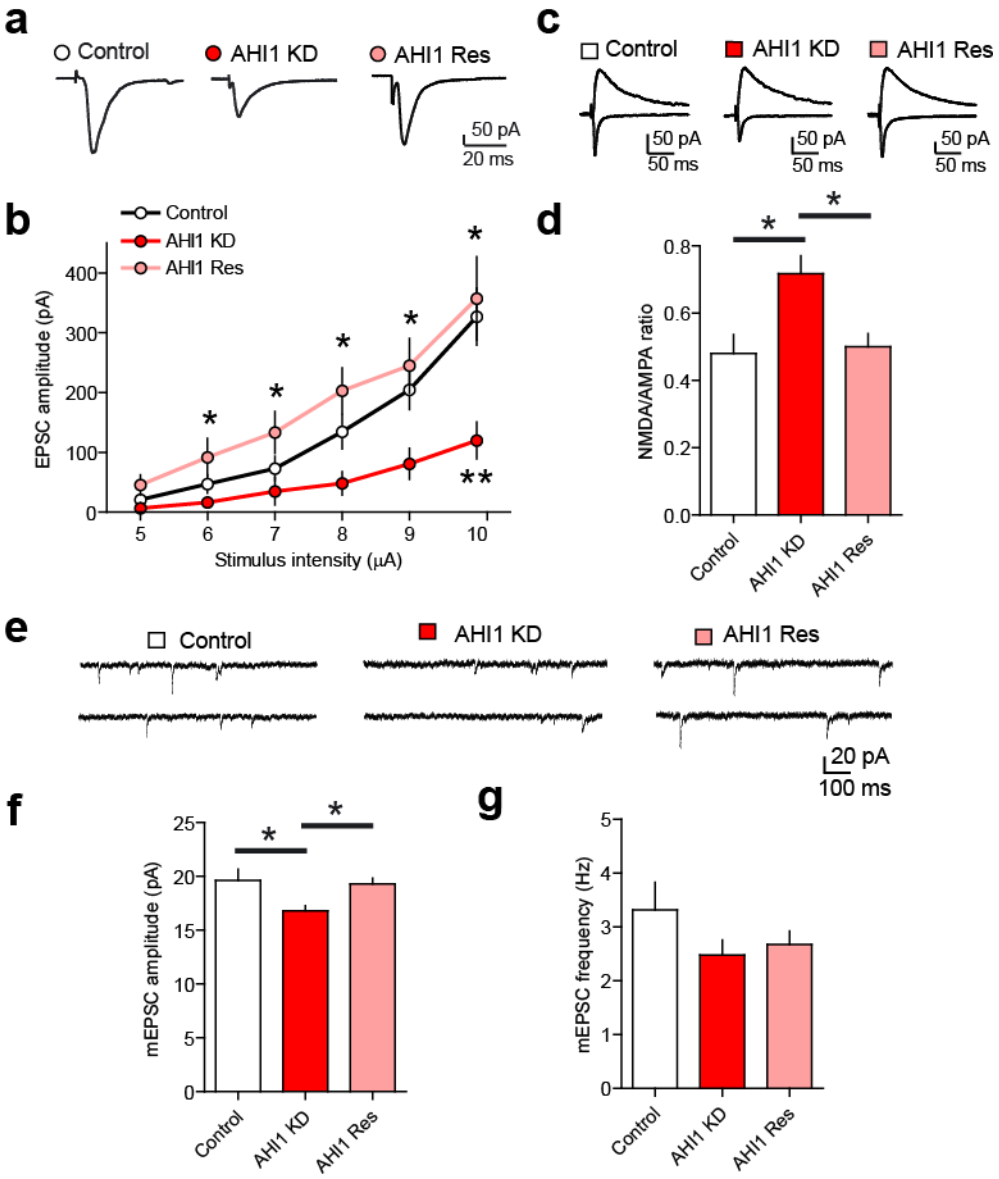

Figure 9 | AHI1-knockdown decreases excitatory synaptic transmission in layer II/III pyramidal cells of the mPFC.

a, b, Representative traces (a) and average input-output relationships (b) for EPSCs induced by stimulation in the layer II/III of the mPFC in control (white circles, n = 11), AHI1-knockdown (AHI1 KD) (red circles, n = 10) and AHI1-rescue (AHI1-Res) (light red circles, n = 11) pyramidal cells. The holding potential was -70 mV. **c, d,** Representative traces (c) and the average NMDA/AMPA ratio (d) for control (white columns, n = 17), AHI-KD, (red columns, n = 19) and AHI-Res (light red columns, n = 14) pyramidal cells. **e-g,** Sample traces of mEPSC (e) and summary bar graphs showing the mean amplitude (f) and frequency (g) for control (white columns, n = 9), AHI1 KD (red columns, n = 10) and AHI1 Res (light red columns, n = 11) pyramidal cells. **P* < 0.05, ***P* < 0.01 (Dunn test). Error bars show mean + SEM.

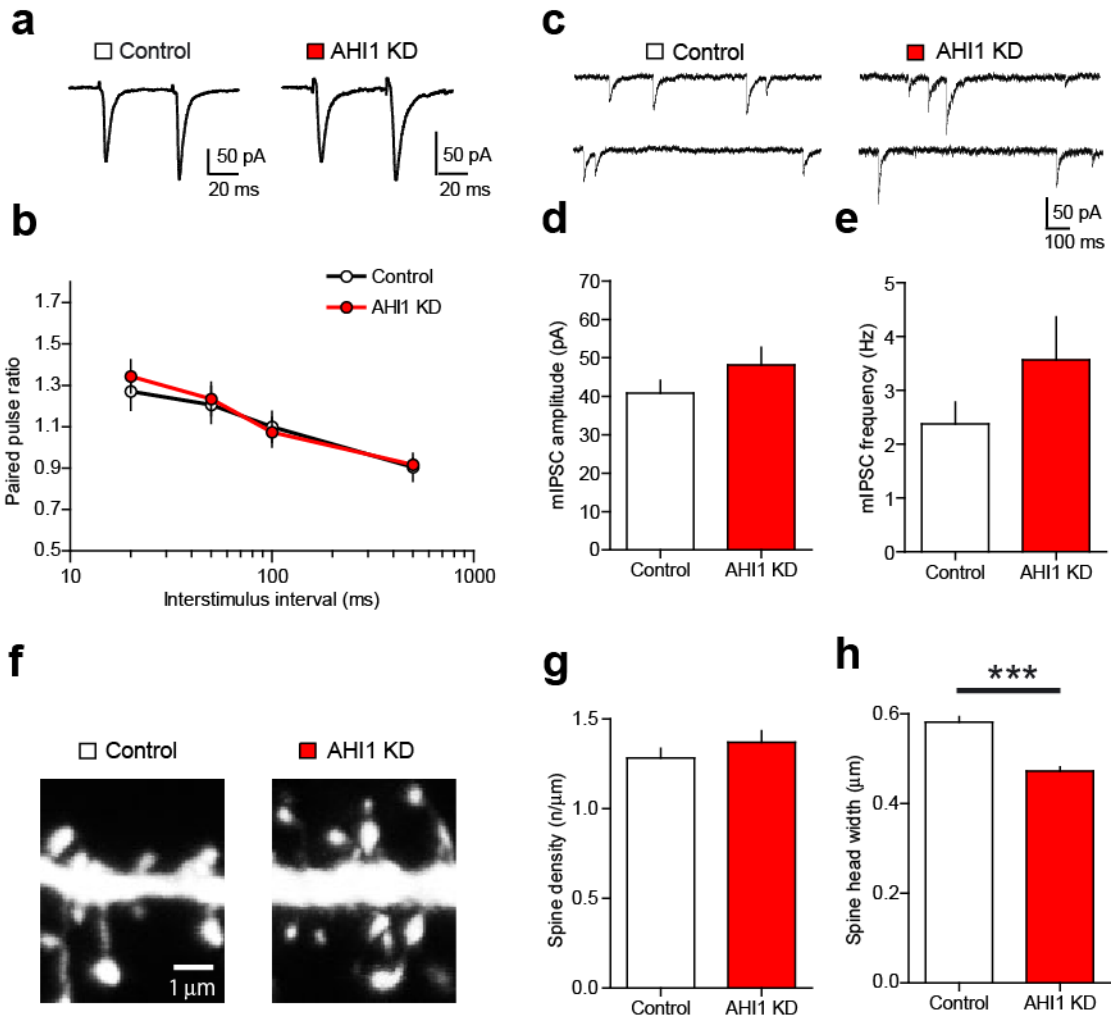

Figure 10 | Effects of AHI1-knockdown in layer II/III pyramidal cells of the mPFC on paired-pulse ratio, mIPSC and spine morphology.

a, b, Representative traces (a) and average values of paired pulse ratio (b) for control (white circles, n = 9) and AHI1-knockdown (AHI1 KD) (red circles, n = 10) pyramidal cells. **c-e,** Sample traces of mIPSC (c) and summary bar graphs showing the mean amplitude (d) and frequency (e) of mIPSC for control (white columns, n = 11) and AHI1 KD (red columns, n = 11) pyramidal cells. **f-h,** Representative images (f) of spine morphology and summary bar graphs showing the mean averaged spine density (g) and spine head width (h) for control (white columns, n = 16) and AHI1 KD (red columns, n = 16) pyramidal cells. ***P < 0.001 (Mann-Whitney U test). Error bars show mean ± SEM.

Mice with AHI1-knockdown in the PFC exhibit impaired social interaction and communication

To test whether mice with AHI-knockdown exhibited ASD-like behaviors, I investigated social interaction, communication, repetitive behaviors and behavioral flexibility. Similar to the mice with CNTNAP2-knockdown, the mice with AHI1-knockdown spent significantly less time around the cage of a stranger mouse than the mice with AHI1-scramble in social interaction analysis (Fig. 11a-c). Moreover, the mice with AHI1-knockdown exhibited significantly smaller number of contact with a freely moving stranger mouse than the mice with AHI1-scramble (Fig. 11d). In the USV analysis, the mice with AHI1-knockdown exhibited a significant reduction in mean duration of calls compared with the mice with AHI1-scramble (Fig. 11e). However, neither repetitive behaviors nor behavioral inflexibility was altered in the mice with AHI1-knockdown compared with the mice with AHI1-scramble (Fig. 12a-c). These results suggest that the mice with AHI1-knockdown in the PFC show impaired social interaction and abnormal communication.

To examine whether AHI1-knockdown in the PFC caused other behavioral abnormalities, I performed a battery of behavior tests. The mice with AHI1-knockdown exhibited decreased depressive behavior, but normal anxiety, locomotor activity and working memory compared with the mice with AHI1-scramble (Fig. 12d-o).

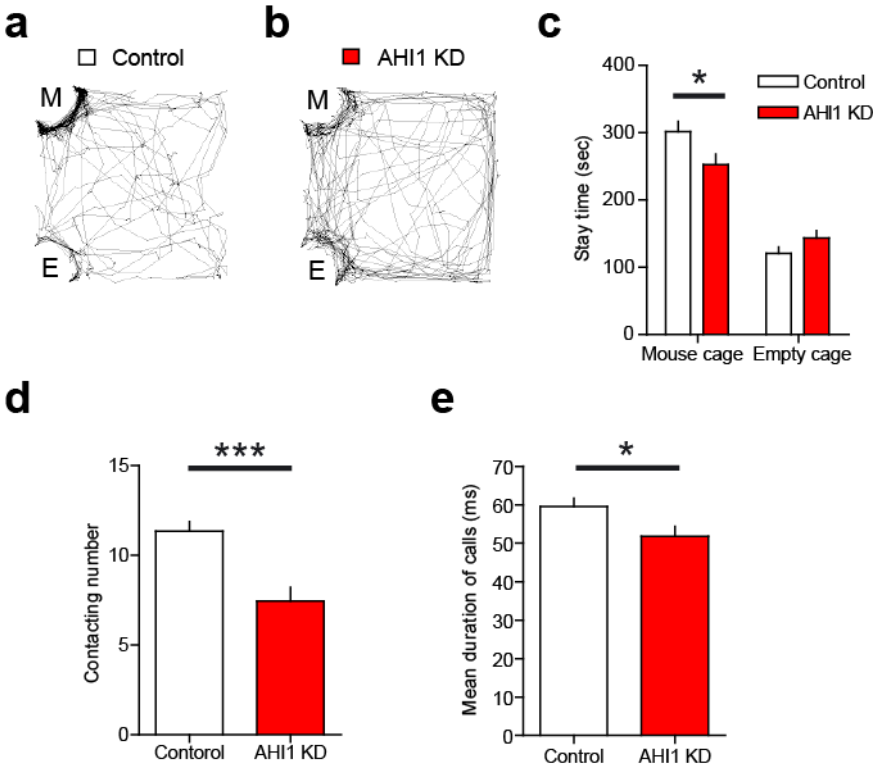

Figure 11 | Impaired social interaction and communication in mice with AHI1-knockdown in the PFC.

a-c, Representative tracks (a, b) and quantification (c) of the results in a and b, as shown by the amount of time spent around the mouse (M) and empty cage (E) in AHI1-scramble (control) (white columns, n = 31) and AHI1 KD (red columns, n = 29) mice. **d,** Number of contacts in control (white column, n = 35) and AHI1 KD (red column, n = 29) mice. **e,** Mean duration of calls in control (white columns, n = 10) and AHI1 KD (red columns, n = 11) pups. *$P < 0.05$, ***$P < 0.001$ (Student's *t* test). Error bars show mean + SEM.

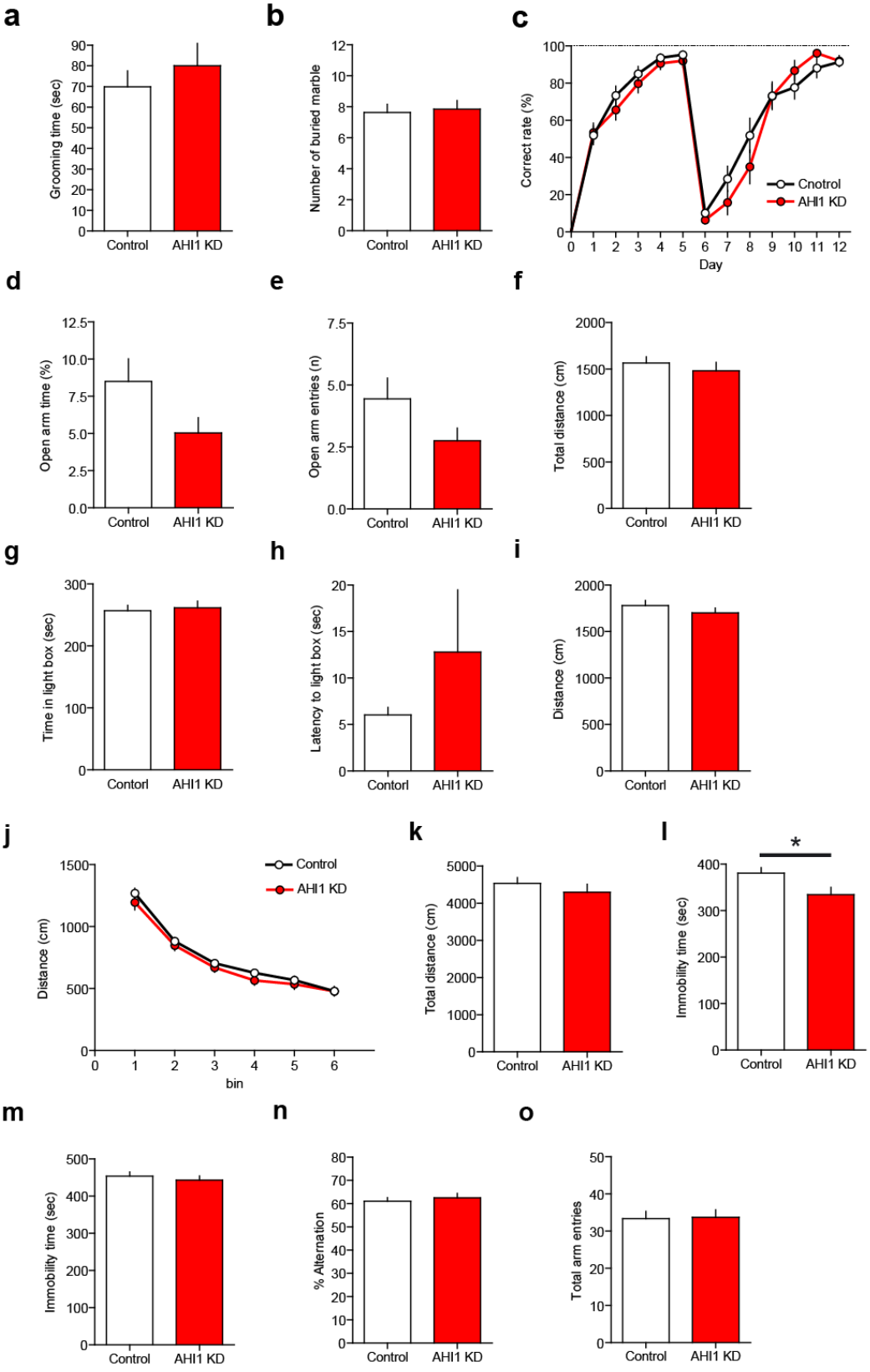
a
Grooming time (sec)
Control
AHI1 KD
b
Number of buried marble
Control
AHI1 KD
c
Correct rate (%)
Day
Cnotrol
AHI1 KD
d
Open arm time (%)
Control
AHI1 KD
e
Open arm entries (n)
Control
AHI1 KD
f
Total distance (cm)
Control
AHI1 KD
g
Time in light box (sec)
Contorl
AHI1 KD
h
Latency to light box (sec)
Contorl
AHI1 KD
i
Distance (cm)
Contorl
AHI1 KD
j
Distance (cm)
bin
Control
AHI1 KD
k
Total distance (cm)
Control
AHI1 KD
l
*
Immobility time (sec)
Control
AHI1 KD
m
Immobility time (sec)
Control
AHI1 KD
n
% Alternation
Control
AHI1 KD
o
Total arm entries
Control
AHI1 KD

Figure 12 | Normal repetitive behaviors, behavioral flexibility, anxiety, locomotor activity and working memory but moderately reduced depressive behavior in mice with AHI1-knockdown in the PFC.

a, Self-grooming test. Total time spent on grooming in control (white column, n = 33) and AHI1 KD (red column, n = 28) mice. **b,** Marble bury test. Number of buried marbles in control (white column, n = 33) and AHI1 KD (red column, n = 28) mice. **c,** Operant reversal learning. Correct rate in control (white column, n = 16) and AHI1 KD (red column, n = 13) mice. **d-e,** Elevated plus maze test. Percentage of time in the open arm (d), the number of open arm entries (e) and total distance travelled (f) in control (white column, n = 34) and AHI1 KD (red column, n = 28) mice. **g-i,** Light/Dark box test. Time in the light box (g), latency to the light box entry (h), and distance travelled (i) in control (white column, n = 34) and AHI1 KD (red column, n = 28) mice. **j,k,** Open field test. Total distance travelled shown in 5 min time bins (j) and during 30 min (k) in control (white column, n = 35) and AHI1 KD (red column, n = 29) mice. **l,** Tail suspension test. Immobility time in control (white column, n = 34) and AHI1 KD (red column, n = 28) mice. **m,** Forced swim test. Immobility time in control (white column, n = 34) and AHI1 KD (red column, n = 28) mice. **n,o,** Y-maze test. Percentage of alternation in control (white column, n = 33) and AHI1 KD (red column, n = 28) mice. $*P < 0.05$ (Student's *t* test). Error bars show mean ± SEM.

CX546 improves social deficits and normalizes reduced excitatory synaptic transmission in mice with AHI1-knockdown in the PFC

The results presented so far suggest that reduced excitatory synaptic transmission is linked to ASD-like behaviors in mice with CNTNAP2 or AHI1 knockdown in the PFC. To further test this possibility, I used the ampakine CX546, a positive allosteric modulator of AMPA receptors. Ampakine increases open ion channel times to enhance excitatory glutamatergic neurotransmission (Arai and Kessler, 2007). First, I evaluated the effect of CX546 (200 μM) on the excitatory synaptic transmission in AHI1-knockdown pyramidal cells in acute slices. I found that application of CX546 (200 μM) significantly enhanced the mEPSC amplitude in AHI1-knockdown cells compared with application of vehicle (Fig. 13a-c). In contrast, CX546 had no significant effect on the mEPSC amplitude in control cells (Fig. 13a-b). As for the mEPSC frequency, CX546 did not cause significant enhancement in AHI1-knockdown and control cells (Fig. 13a and c). I found that the decay time of mEPSC became significantly longer after the CX546 treatment in both control and AHI1-knockdown cells (Fig. 13e and f). These results suggest that CX546 restores the impaired excitatory synaptic transmission in AHI1-knockdown cells.

Finally, I examined whether CX546 could rescue the abnormal behaviors found in mice with AHI1-knockdown in the PFC. I found that injection of CX546 (25 mg/kg) into the mice with AHI1-knockdown significantly improved their scores in both social novelty and reciprocal social interaction tests when compared with vehicle injection (Fig. 14c, d, e and g). In contrast, injection of CX546 (25 mg/kg) into the mice with AHI1-scramble had no significant effects on their social interaction (Fig. 14a, b, e and g). CX546 (25 mg/kg) did not affect stay time around the empty cage in the mice with

AHI1- scramble and AHI1- knockdown (Fig. 14f). These results suggest that reduced excitatory synaptic transmission is a main cause of impaired social interaction in the mice with AHI1-knockdown in the PFC. In addition, these data may provide a basis for potential therapeutic use of Ampakines for impaired social interaction.

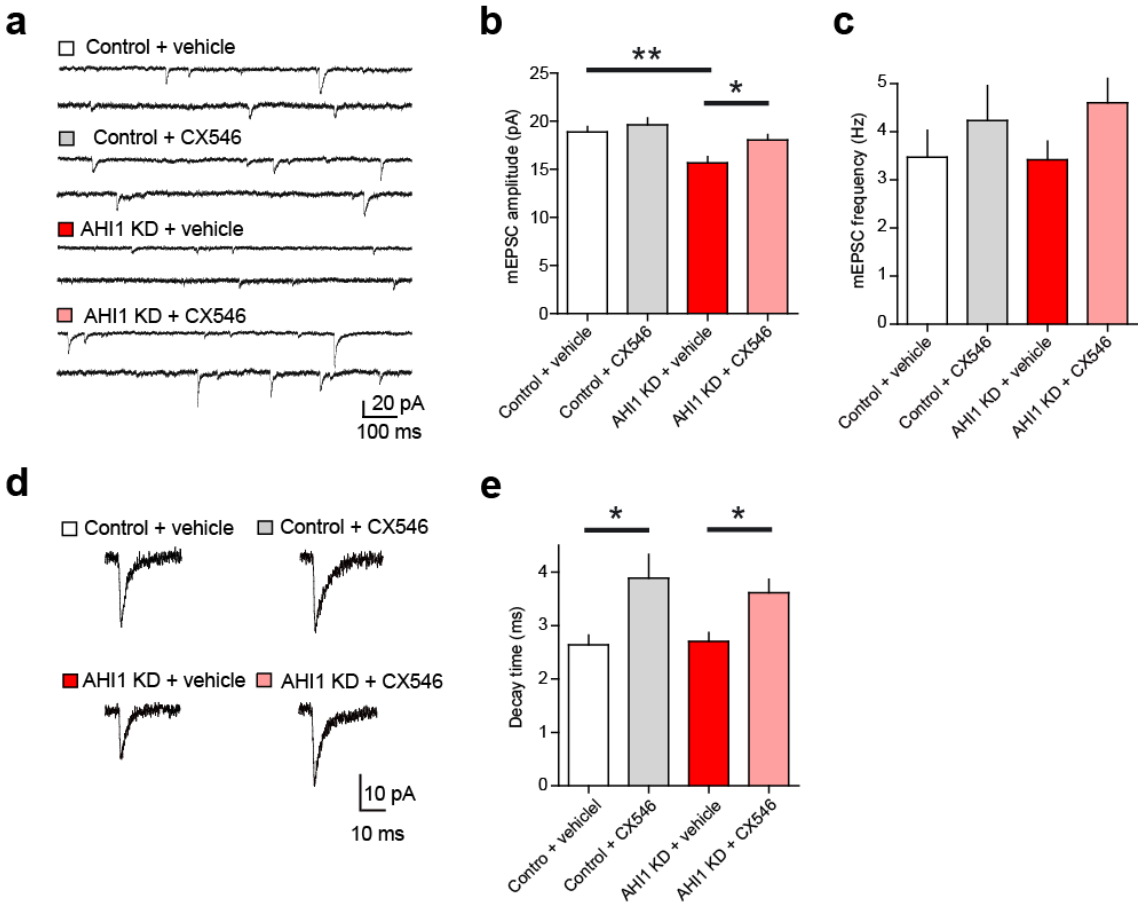

Figure 13 | CX546 normalizes reduced excitatory synaptic transmission in layer II/III pyramidal cells of the mPFC.

a-c, Sample traces of mEPSC (a) and summary bar graphs showing the mean amplitude (b) and frequency (c) of mEPSC for vehicle-treated control (control + vehicle) (white columns, n = 12), CX546-treated control (control + CX546) (gray columns, n = 12), vehicle-treated AHI1 KD (AHI1 KD + vehicle) (red columns, n = 15) and CX546-treated AHI1 KD (AHI1 KD + CX546) (light red columns, n = 15) cells. $^{**}P < 0.01$, $^{*}P < 0.05$ (Dunn test). **d-e,** Sample traces of mEPSC (d) and summary bar graphs showing the mean decay time constant of mEPSC (e) for control + vehicle (white columns, n = 12), control + CX546 (gray columns, n = 12), AHI1 KD + vehicle (red columns, n = 15) and AHI1 KD + CX546 (light red columns, n = 15) cells. $^{*}P < 0.05$ (Dunn test). Error bars show mean + SEM.

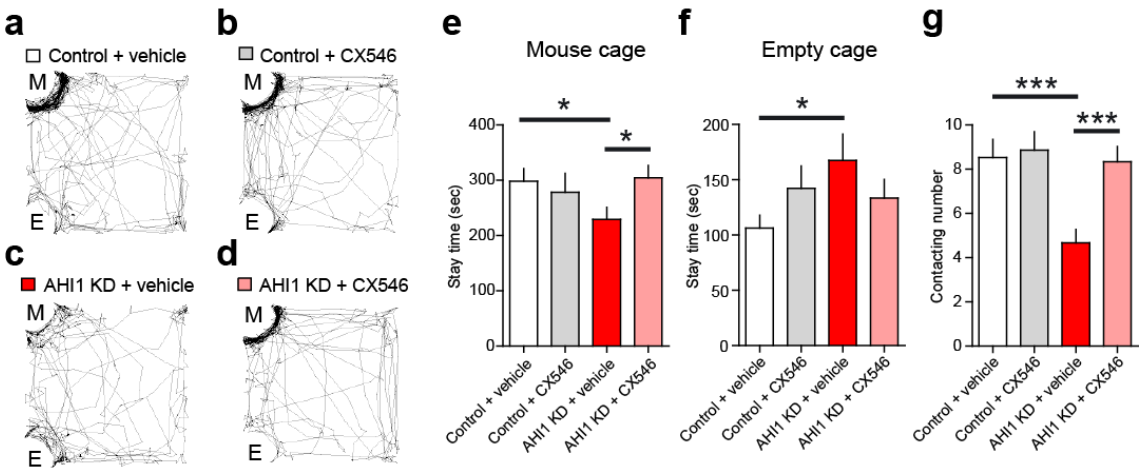

Figure 14 | CX546 improves social deficits in mice with AHI1-knockdown in the PFC.

a-f, Representative tracks (a-d) and quantification (e, f) of the results in a, b, c and d as shown by the amount of time spent around the mouse (M) and empty cage (E) in vehicle-treated control (control + vehicle) (white columns, n = 20), CX546-treated control (control + CX546) (gray columns, n = 20), vehicle-treated AHI1 KD (AHI1 KD + vehicle) (red columns, n = 24) and CX546-treated AHI1 KD (AHI1 KD + CX546) (light red columns, n = 25) mice. $*P < 0.05$ (Student's *t* test). **g,** Number of contacts in control + vehicle (white columns, n = 26), control + CX546 (gray columns, n = 23), AHI1 KD + vehicle (red columns, n = 25) and AHI1 KD + CX546 (light red columns, n = 26) mice. $***P < 0.001$ (Student's *t* test). Error bars show mean + SEM.

Discussion

Recent studies have identified numerous genes whose mutations are found in patients with ASD (Abrahams and Geschwind, 2008; Devlin and Scherer, 2012). However, roles of such genes in synapse development and function, their contributions to ASD-like behaviors, and brain regions where they function remain largely unknown. Many ASD mouse models have been developed by genetic manipulation (knockout, knockin and transgenic) to study the mechanisms underlying ASD (Tabuchi et al., 2007; Chao et al., 2010; Peça et al., 2011; Han et al., 2012; Schmeisser et al., 2012; Won et al., 2012; Santini et al., 2013; Gkogkas et al., 2013; Chung et al., 2015; Liang et al., 2015). The results from the analyses of these ASD mouse models suggest pathways including aberrant mRNA translation, the abnormal function of NMDA receptors, and the imbalance between excitation and inhibition as major causes of ASD (Delorme et al., 2013; Ebert et al., 2013; Lee et al., 2015). However, it remains to be elucidated whether each ASD-associated gene functions in its own specific pathway or multiple genes operate in one of a few common pathways for the pathogenesis of ASD. To tackle this difficult problem, methods are required which enable us to examine roles of ASD-associated genes quickly and easily. The roles of Disrupted-in-Schizophrenia-1 (DISC1) gene of layer II/III pyramidal cells of the PFC in schizophrenia-related behaviors have been investigated by a knockdown method using in utero electroporation (Niwa et al., 2010； Hayashi-Takagi et al., 2014). However, it is unknown whether the same method can utilize ASD-like behaviors including social interaction, communication, and stereotyped and repetitive behaviors. I optimized the technique for ASD-like behaviors and established an assay system by which the roles of

ASD-associated genes in synaptic development and function can be examined in the PFC, and possible causal relationship between synaptic dysfunction in the PFC and ASD-like behaviors can be pursued. Since my methods utilize microRNA-mediated knockdown of genes of interest specifically in layer II/III pyramidal cells of the PFC by means of in utero electroporation, they are faster, easier and less expensive than those which use brain-region or cell-type specific conditional knockout mice. Furthermore, since my methods allow deletion of a targeted gene in only a subset of layer II/III pyramidal cells of the PFC, a causal link between the lack of the gene in layer II/III pyramidal cells of the PFC and ASD-like behavior can be elucidated unequivocally. With these technical advantages of this system, it will be possible to characterize and classify many ASD-related genes of unknown function, to elucidate novel mechanisms underlying ASD-like phenotypes, and thus to facilitate the research on the pathophysiology of ASD.

Several researchers have investigated brain regions which are involved in ASD-like behaviors. For example, optogenetic activation of mPFC leads to social interaction deficits (Yizhar et al., 2011). Disturbance of neuroligin-3 function in medium spiny neurons expressing D1-dopamine receptors of the striatum leads to enhanced repetitive behaviors (Rothwell et al., 2014). Dysfunction of Tsc1 in cerebellar Purkinje cells displays ASD-like behaviors, including social interaction and communication, and stereotyped and repetitive behaviors (Peter et al., 2012). I found that knockdown of either CNTNAP2 or AHI1 in layer II/III pyramidal cells of the mouse PFC caused impairment in social interaction and communication (Fig. 5 and 11) but no change in repetitive behaviors and behavioral inflexibility (Fig. 6a-c and 12a-c). These results should be interpreted with the limitation of the present experimental condition that gene

function in the PFC was not completely disrupted and only a part of layer II/III pyramidal cells in the PFC were affected by RNAi knockdown. Nevertheless, the results of the present study unequivocally indicate that the PFC is important for social interaction and communication. Taken together, the results of the previous studies and the present study collectively suggest that ASD-like behaviors are caused by the abnormalities of several different brain regions. It will be of interest to investigate the interaction of multiple areas and the circuit in which social interaction and communication, and stereotyped and repetitive behaviors are controlled.

I disclosed new roles of AHI1 as a regulator gene of synaptic development and function (Fig. 9 and 10). It remains unknown how AHI1 controls excitatory synaptic transmission. AHI1 interacts with huntingtin-associated protein 1 (HAP1) and the deletion of AHI1 results in reduced HAP1 protein in the mouse brain (Sheng et al., 2008; Xu et al., 2010). In addition, a previous study on cortical neurons suggests that HAP1 plays important roles in AMPA receptor trafficking and function through the kinesin motor protein 5 which contributes to transport of AMPA receptors (Mandal et al., 2011). Because my results suggest that AHI1 regulates AMPAR-mediated synaptic transmission (Fig. 9), it is possible that disturbance of AHI1 impairs HAP1 function and causes impaired AMPA receptor trafficking and function.

Although mutation of AHI1 in patients with ASD has been reported, roles of AHI1 in social interaction, communication, and stereotyped and repetitive behaviors remain largely unknown. A previous study reports that social interaction time is significantly increased in AHI1 heterozygous knockout mice (Lotan et al., 2014). In contrast, mice with AHI1-knockdown in the PFC showed impaired social interaction and communication (Fig. 11). One possibility for the apparent discrepancy in the phenotype

between AHI1heterozygous knockout mice and mice with AHI1 knockdown mice may be the difference in the level of anxiety between the two mouse lines, because social behavior is closely linked to anxiety. Mice with AHI1-knockdown in the PFC showed normal anxiety (Fig. 12d-i) whereas AHI1 heterozygous knockout mice exhibited decreased anxiety (Lotan et al., 2014). The low anxiety level in AHI1 heterozygous knockout mice may have led to an increase in social interaction.

Knockdown of either, CNTNAP2 or AHI1 in layer II/III pyramidal cells of the mouse PFC resulted in deficit of excitatory synaptic transmission and social interaction and communication (Fig. 4, 5, 9 and 11). The CNTNAP2 and AHI1 microRNAs designed in this study suppressed the well-characterized splice variant (long form) of each gene. However, it should be noted that the function of other splice variants (short form) remains unclear. In addition, CX546 rescued reduced excitatory synaptic transmission and social interaction deficits in mice with AHI-knockdown (Fig. 13 and 14). These results collectively suggest that deficit of excitatory synaptic transmission in the PFC is a main cause of social interaction and communication. Diverse synaptic dysfunctions are reported to contribute to the etiology of ASD (Pardo et al., 2005; Delorme et al., 2013; Ebert and Greenberg, 2013) and apparently opposite synaptic defects are reported in different ASD mouse models (Tabuchi et al., 2007; Chao et al., 2010; Peça et al., 2011; Han et al., 2012; Schmeisser et al., 2012; Santini et al., 2013; Gkogkas et al., 2013; Han et al., 2014; Chung, et al., 2015; Liang et al., 2015). For instance, Shank2 knockout mice (lacking exons 6 and 7) show reduced NMDAR function (Won et al., 2012) whereas another line of Shank2 knockout mice (lacking exon 7) and IRSp53 knockout mice show increased NMDAR function (Schmeisser, et al., 2012; Chung, et al., 2015). An increase in the inhibitory synaptic transmission was observed in

neuroligin-3 knock-in R451C mice (Tabuchi et al., 2007) whereas a reduction in inhibitory synaptic transmission was reported in BTBR mice (Han et al., 2014). Taken together, these results suggest that individual patients with ASD may have change in synaptic function in specific directions depending on the genes involved. To provide effective treatment for patients with ASD, roles of ASD-related genes of unknown function should be revealed and categorized into groups based on the nature of synaptic defect.

In conclusion, I used the methods that enable researchers to examine whether ASD susceptibility genes influence the development and function of synapses in the PFC and ASD-like behaviors (Fig. 4 and 5), and found that knockdown of either CNTNAP2 or AHI1 in layer II/III pyramidal cells of the mouse PFC impaired excitatory synaptic transmission and led to impairment of social interaction and communication, the two core symptoms of ASD-like behaviors in mice (Fig. 4, 5, 9 and 11). These results suggest that excitatory synaptic transmission in layer II/III pyramidal cells of the PFC mediates core symptom of ASD.

Acknowledgments

I would like to express my sincere gratitude to Professor Masanobu Kano for supervising me during the graduate course. I am deeply grateful to Dr. Naohumi Uesaka for warm and helpful advice and support throughout the course of this study. I also thank Dr. K. Sakoori for helpful advice for behaviors, Dr. T. Nakazawa for helpful advice for spine morphology, Dr. T. Watanabe for helpful advice for vector constructs, Drs. K. Kitamura, Y Hashimotodani and Y. Sugaya for helpful discussions and K. Matsuyama, M. Sekiguchi and M. Baba for technical assistance.

Reference

1. Abrahams BS & Geschwind DH. Advances in autism genetics: on the threshold of a new neurobiology. *Nat. Rev. Genet.* **9,** 341–355 (2008).
2. Ade KK, Janssen MJ, Ortinski PI & Vicini S. Differential tonic GABA conductances in striatal medium spiny neurons. *J Neurosci* **28,** 1185-1197 (2008)
3. Alvarez Retuerto AI, Cantor RM, Gleeson JG, Ustaszewska A, Schackwitz WS, Pennacchio LA, Geschwind DH. Association of common variants in the Joubert syndrome gene (AHI1) with autism. *Hum Mol Genet* **17,** 3887–3896 (2008)
4. Amodio DM & Frith CD. Meeting of minds: the medial frontal cortex and social cognition. *Nat Rev Neurosci* **7,** 268-277 (2006)
5. Anderson GR, Galfin T, Xu W, Aoto J, Malenka RC, Südhof TC. Candidate autism gene screen identifies critical role for cell-adhesion molecule CASPR2 in dendritic arborization and spine development. *Proc Natl Acad Sci U S A* **109,** 18120-18125 (2012)
6. Arai AC & Kessler M. Pharmacology of ampakine modulators: from AMPA receptors to synapses and behavior. *Curr Drug Targets* **8**,583-602 (2007)
7. Chao HT, Chen H, Samaco RC, Xue M, Chahrour M, Yoo J, Neul JL, Gong S, Lu HC, Heintz N, Ekker M, Rubenstein JL, Noebels JL, Rosenmund C, Zoghbi HY.

Dysfunction in GABA signalling mediates autism-like stereotypies and Rett syndrome phenotypes. *Nature* **68,** 263-269 (2010)

8. Chung W, Choi SY, Lee E, Park H, Kang J, Park H, Choi Y, Lee D, Park SG, Kim R, Cho YS, Choi J, Kim MH, Lee JW, Lee S, Rhim I, Jung MW, Kim D, Bae YC, Kim E. Social deficits in IRSp53 mutant mice improved by NMDAR and mGluR5 suppression. *Nat Neurosci* **18,** 435-443 (2015)
9. Courchesne E, Mouton PR, Calhoun ME, Semendeferi K, Ahrens-Barbeau C, Hallet MJ, Barnes CC, Pierce K. Neuron number and size in prefrontal cortex of children with autism. *JAMA* **306,** 2001-2010 (2011)
10. Delorme R, Ey E, Toro R, Leboyer M, Gillberg C, Bourgeron T. Progress toward treatments for synaptic defects in autism. *Nat Med* **19,** 685-694 (2013)
11. Devlin B & Scherer SW. Genetic architecture in autism spectrum disorder. *Curr. Opin. Genet. Dev.* **22**, 229–237 (2012).
12. Ding JB, Oh WJ, Sabatini BL & Gu C. Semaphorin 3E-Plexin-D1 signaling controls pathway-specific synapse formation in the striatum. *Nat Neurosci* **15,** 215-223 (2011)
13. Dixon-Salazar T, Silhavy JL, Marsh SE, Louie CM, Scott LC, Gururaj A, Al-Gazali L, Al-Tawari AA, Kayserili H, Sztriha L, Gleeson JG. Mutations in the AHI1 gene,

encoding jouberin, cause Joubert syndrome with cortical polymicrogyria. *Am. J. Hum. Genet.* **75,** 979–987 (2004).

14. Dumitriu D, Rodriguez A. & Morrison JH. High-throughput, detailed, cell-specific neuroanatomy of dendritic spines using microinjection and confocal microscopy. *Nature Protocols* **6,** 1391–1411 (2011).

15. Ebert DH & Greenberg ME. Activity-dependent neuronal signalling and autism spectrum disorder. *Nature* **49,** 327-337 (2013)

16. Ferland RJ, Eyaid W, Collura RV, Tully LD, Hill RS, Al-Nouri D, Al-Rumayyan A, Topcu M, Gascon G, Bodell A, Shugart YY, Ruvolo M, Walsh CA. Abnormal cerebellar development and axonal decussation due to mutations in AHI1 in Joubert syndrome. *Nat. Genet.* **36,** 1008–1013 (2004).

17. Gkogkas CG, Khoutorsky A, Ran I, Rampakakis E, Nevarko T, Weatherill DB, Vasuta C, Yee S, Truitt M, Dallaire P, Major F, Lasko P, Ruggero D, Nader K, Lacaille JC, Sonenberg N. Autism-related deficits via dysregulated eIF4E-dependent translational control. *Nature* **493,** 371-377 (2013)

18. Han S, Tai C, Westenbroek RE, Yu FH, Cheah CS, Potter GB, Rubenstein JL, Scheuer T, de la Iglesia HO, Catterall WA. Autistic-like behaviour in Scn1a$^{+/-}$ mice and rescue by enhanced GABA-mediated neurotransmission. *Nature* **489,** 385-390

(2012)

19. Han S, Tai C, Jones CJ, Scheuer T, Catterall WA. Enhancement of inhibitory neurotransmission by GABAA receptors having α2,3-subunits ameliorates behavioral deficits in a mouse model of autism. *Neuron* **81,** 1282-1289 (2014)
20. Hatayama M, Ishiguro A, Iwayama Y, Takashima N, Sakoori K, Toyota T, Nozaki Y, Odaka YS, Yamada K, Yoshikawa T, Aruga J. Zic2 hypomorphic mutant mice as a schizophrenia model and ZIC2 mutations identified in schizophrenia patients. Sci Rep **1**, 16 (2011)
21. Hayashi-Takagi A, Araki Y, Nakamura M, Vollrath B, Duron SG, Yan Z, Kasai H, Huganir RL, Campbell DA, Sawa A. PAKs inhibitors ameliorate schizophrenia-associated dendritic spine deterioration in vitro and in vivo during late adolescence. *Proc Natl Acad Sci U S A* **111**, 6461-6466 (2014)
22. Holroyd S, Reiss, AL & Bryan RN. Autistic features in Joubert syndrome: a genetic disorder with agenesis of the cerebellar vermis. *Biol Psychiatry* **29,** 287-294 (1991)
23. Jurgensen S & Castillo PE. Selective Dysregulation of Hippocampal Inhibition in the Mouse Lacking Autism Candidate Gene CNTNAP2. *J Neurosci* **35,**14681-146817 (2015)
24. Kaidanovich-Beilin O, Lipina TV, Takao K, van Eede M, Hattori S, Laliberté C, Khan M, Okamoto K, Chambers JW, Fletcher PJ, MacAulay K, Doble BW,

Henkelman M, Miyakawa T, Roder J, Woodgett JR. Abnormalities in brain structure and behavior in GSK-3alpha mutant mice. *Mol Brain* **2**, 35 (2009)

25. Kim CS, Chang PY and Johnston D. Enhancement of dorsal hippocampal activity by knockdown of HCN1 channels leads to anxiolytic- and antidepressant-like behaviors. *Neuron* **75**, 503-516 (2012)
26. Lee EJ, Choi SY, Kim E. NMDA receptor dysfunction in autism spectrum disorders. *Curr Opin Pharmacol* **20,** 8-13 (2015)
27. Li K, Zhou T, Liao L, Yang Z, Wong C, Henn F, Malinow R, Yates JR 3rd, Hu H. βCaMKII in lateral habenula mediates core symptoms of depression. *Science* **341**, 1016-1020 (2013)
28. Liang J, Xu W, Hsu YT, Yee AX, Chen L, Südhof TC. Conditional neuroligin-2 knockout in adult medial prefrontal cortex links chronic changes in synaptic inhibition to cognitive impairments. *Mol Psychiatry* **20,** 850-859 (2015)
29. Lotan A, Lifschytz T, Slonimsky A, Broner EC, Greenbaum L, Abedat S, Fellig Y, Cohen H, Lory O, Goelman G, Lerer B. Neural mechanisms underlying stress resilience in Ahi1 knockout mice: relevance to neuropsychiatric disorders. *Mol Psychiatry.* **19,** 243-252 (2014)
30. Maejima T, Oka S, Hashimotodani Y, Ohno-Shosaku T, Aiba A, Wu D, Waku K,

Sugiura T, Kano M. Synaptically driven endocannabinoid release requires Ca2+-assisted metabotropic glutamate receptor subtype 1 to phospholipase Cbeta4 signaling cascade in the cerebellum. *J Neurosci* **25,** 6826-6835 (2005)

31. Mandal M, Wei J, Zhong P, Cheng J, Duffney LJ, Liu W, Yuen EY, Twelvetrees AE, Li S, Li XJ, Kittler JT, Yan Z. Impaired alpha-amino-3-hydroxy-5-methyl-4-isoxazolepropionic acid (AMPA) receptor trafficking and function by mutant huntingtin. J Biol Chem **286,** 33719-33728 (2011)
32. Mikuni T, Uesaka N, Okuno H, Hirai H, Deisseroth K, Bito H, Kano M. Arc/Arg3.1 is a postsynaptic mediator of activity-dependent synapse elimination in the developing cerebellum. *Neuron* **78,** 1024-1035 (2013)
33. Narushima M, Hashimoto K, Kano M. Endocannabinoid-mediated short-term suppression of excitatory synaptic transmission to medium spiny neurons in the striatum. *Neurosci Res* **54**, 159-164 (2006)
34. Niwa H, Yamamura K, Miyazaki J. Efficient selection for high-expression transfectants with a novel eukaryotic vector. *Gene* **108,** 193-199. (1991)
35. Niwa M, Kamiya A, Murai R, Kubo K, Gruber AJ, Tomita K, Lu L, Tomisato S, Jaaro-Peled H, Seshadri S, Hiyama H, Huang B, Kohda K, Noda Y, O'Donnell P, Nakajima K, Sawa A, Nabeshima T. Knockdown of DISC1 by in utero gene transfer

disturbs postnatal dopaminergic maturation in the frontal cortex and leads to adult behavioral deficits. *Neuron* **65,** 480-489 (2010)

36. Ozonoff S, Williams BJ, Gale S, & Miller JN. Autism and autistic behavior in Joubert syndrome. *J Child Neurol* **14,** 636-641 (1999)
37. Pardo CA, Vargas DL & Zimmerman AW. Immunity, neuroglia and neuroinflammation in autism. *Int Rev Psychiatry* **17,** 485-495 (2005)
38. Peça J, Feliciano C, Ting JT, Wang W, Wells MF, Venkatraman TN, Lascola CD, Fu Z, Feng G. Shank3 mutant mice display autistic-like behaviours and striatal dysfunction. *Nature* **472,** 437–442 (2011).
39. Peñagarikano O, Abrahams BS, Herman EI, Winden KD, Gdalyahu A, Dong H, Sonnenblick LI, Gruver R, Almajano J, Bragin A, Golshani P, Trachtenberg JT, Peles E, Geschwind DH. Absence of CNTNAP2 leads to epilepsy, neuronal migration abnormalities, and core autism-related deficits. *Cell* **147**, 235–246 (2011)
40. Peñagarikano O & Geschwind, D.H. What does CNTNAP2 reveal about autism spectrum disorder? *Trends Mol Med.* **18**, 156–163 (2012)
41. Poliak S, Gollan L, Martinez R, Custer A, Einheber S, Salzer JL, Trimmer JS, Shrager P, Peles E. Caspr2, a new member of the neurexin superfamily, is localized at the juxtaparanodes of myelinated axons and associates with K+ channels. *Neuron*

24, 1037–1047 (1999)

42. Poliak S, Salomon D, Elhanany H, Sabanay H, Kiernan B, Pevny L, Stewart CL, Xu X, Chiu SY, Shrager P, Furley AJ, Peles E. Juxtaparanodal clustering of Shaker-like K+ channels in myelinated axons depends on Caspr2 and TAG-1. *J Cell Biol.* **162,** 149-160 (2003)

43. Rothwell PE, Fuccillo MV, Maxeiner S, Hayton SJ, Gokce O, Lim BK, Fowler SC, Malenka RC, Südhof TC. Autism-associated neuroligin-3 mutations commonly impair striatal circuits to boost repetitive behaviors. *Cell* **158,** 198-212 (2014)

44. Saito, T. In vivo electroporation in the embryonic mouse central nervous system. *Nat Protoc* **1,** 1552-1558 (2006)

45. Santini E, Huynh TN, MacAskill AF, Carter AG, Pierre P, Ruggero D, Kaphzan H, Klann E. Exaggerated translation causes synaptic and behavioural aberrations associated with autism. *Nature* **493,** 411-415 (2013)

46. Scearce-Levie K., Roberson ED, Gerstein H, Cholfin JA, Mandiyan VS, Shah NM, Rubenstein JL, Mucke L. Abnormal social behaviors in mice lacking Fgf17. *Genes Brain Behav* **7**, 344-354 (2008)

47. Schmeisser MJ, Ey E, Wegener S, Bockmann J, Stempel AV, Kuebler A, Janssen AL, Udvardi PT, Shiban E, Spilker C, Balschun D, Skryabin BV, Dieck St, Smalla KH,

Montag D, Leblond CS, Faure P, Torquet N, Le Sourd AM, Toro R, Grabrucker AM, Shoichet SA, Schmitz D, Kreutz MR, Bourgeron T, Gundelfinger ED, Boeckers TM. Autistic-like behaviours and hyperactivity in mice lacking ProSAP1/Shank2. *Nature* **486,** 256-260 (2012)

48. Sheng G, Xu X, Lin YF, Wang CE, Rong J, Cheng D, Peng J, Jiang X, Li SH, Li XJ. Huntingtin-associated protein 1 interacts with Ahi1 to regulate cerebellar and brainstem development in mice. *J Clin Invest* **18**, 2785-2795 (2008)
49. Silverman JL, Oliver CF, Karras MN, Gastrell PT & Crawley JN. AMPAKINE enhancement of social interaction in the BTBR mouse model of autism. *Neuropharmacology* **64,** 268-282 (2013)
50. Tabuchi K, Blundell J, Etherton MR, Hammer RE, Liu X, Powell CM, Südhof TC. A neuroligin-3mutation implicated in autism increases inhibitory synaptic transmission in mice. *Science* **318,** 71–76 (2007).
51. Takashima N, Odaka YS, Sakoori K, Akagi T, Hashikawa T, Morimura N, Yamada K, Aruga J. Impaired cognitive function and altered hippocampal synapse morphology in mice lacking Lrrtm1, a gene associated with schizophrenia. *PLoS One* **6**, e22716 (2011)
52. Tsai PT, Hull C, Chu Y, Greene-Colozzi E, Sadowski AR, Leech JM, Steinberg J,

Crawley JN, Regehr WG, Sahin M. Autistic-like behaviour and cerebellar dysfunction in Purkinje cell Tsc1 mutant mice. *Nature* **488,** 647-651 (2012)

53. Uesaka N, Mikuni T, Hashimoto K, Hirai H, Sakimura K, Kano M. Organotypic coculture preparation for the study of developmental synapse elimination in mammalian brain. *J Neurosci* **32,** 11657-11670 (2012)
54. Uesaka N, Uchigashima M, Mikuni T, Nakazawa T, Nakao H, Hirai H, Aiba A, Watanabe M, Kano M. Retrograde semaphorin signaling regulates synapse elimination in the developing mouse brain. *Science* **344,** 1020-1023 (2014)
55. Varea O, Martin-de-Saavedra MD, Kopeikina KJ, Schürmann B, Fleming HJ, Fawcett-Patel JM, Bach A, Jang S, Peles E, Kim E, Penzes P. Synaptic abnormalities and cytoplasmic glutamate receptor aggregates in contactin associated protein-like 2/Caspr2 knockout neurons. *Proc Natl Acad Sci U S A* **112,** 6176-6181 (2015)
56. Wang F, Zhu J, Zhu H, Zhang Q, Lin Z, Hu H. Bidirectional control of social hierarchy by synaptic efficacy in medial prefrontal cortex. *Science* **334**, 693-697 (2011)
57. Won H, Lee HR, Gee HY, Mah W, Kim JI, Lee J, Ha S, Chung C, Jung ES, Cho YS, Park SG, Lee JS, Lee K, Kim D, Bae YC, Kaang BK, Lee MG, Kim E. Autistic-like social behaviour in Shank2-mutant mice improved by restoring NMDA receptor function. *Nature* **486,** 261-265 (2012)

58. Xu X, Yang H, Lin YF, Li X, Cape A, Ressler KJ, Li S, Li XJ. Neuronal Abelson helper integration site-1 (Ahi1) deficiency in mice alters TrkB signaling with a depressive phenotype. *Proc Natl Acad Sci U S A* **107,** 19126-19131 (2010)

59. Yizhar O, Fenno LE, Prigge M, Schneider F, Davidson TJ, O'Shea DJ, Sohal VS, Goshen I, Finkelstein J, Paz JT, Stehfest K, Fudim R, Ramakrishnan C, Huguenard JR, Hegemann P, Deisseroth K. Neocortical excitation/inhibition balance in information processing and social dysfunction. *Nature* **477,** 171–178 (2011).